DEVELOPMENTAL NEUROSCIENCE

Trappc9 deficiency in mice impairs learning and memory by causing imbalance of dopamine D1 and D2 neurons

Yuting Ke[1,2], Meiqian Weng[3], Gaurav Chhetri[1], Muhammad Usman[1], Yan Li[1], Qing Yu[4], Yingzhuo Ding[1], Zejian Wang[1], Xiaolong Wang[1], Pinky Sultana[1], Marian DiFiglia[2], Xueyi Li[1,2]*

Genetic mutations in the gene encoding transport protein particle complex 9 (trappc9), a subunit of TRAPP that acts as a guanine nucleotide exchange factor for rab proteins, cause intellectual disability with brain structural malformations by elusive mechanisms. Here, we report that trappc9-deficient mice exhibit a broad range of behavioral deficits and postnatal delay in growth of the brain. Contrary to volume decline of various brain structures, the striatum of trappc9 null mice was enlarged. An imbalance existed between dopamine D1 and D2 receptor containing neurons in the brain of trappc9-deficient mice; pharmacological manipulation of dopamine receptors improved performances of trappc9 null mice to levels of wild-type mice on cognitive tasks. Loss of trappc9 compromised the activation of rab11 in the brain and resulted in retardation of endocytic receptor recycling in neurons. Our study elicits a pathogenic mechanism and a potential treatment for trappc9-linked disorders including intellectual disability.

INTRODUCTION

Intellectual disability (ID) is a common neurodevelopmental disorder that impairs the ability of affected persons to understand, learn, and apply daily social and practical skills. ID is often associated with other neurodevelopmental conditions, e.g., autism spectrum disorder (ASD) (*1*). Genetic mutations resulting in a loss of transport protein particle (TRAPP) complex 9 (trappc9) occur in families of different ethnic backgrounds and cause moderate to severe ID, delayed speech, delayed walking despite normal motor development, postnatal microcephaly, and variable stereotypic movements, seizure, and obesity (*2*–*9*). Pathologies in the brain of patients with ID with trappc9 mutations include white matter hypoplasia, corpus callosum thinning, and variable atrophy of the cerebellum and certain cerebral cortical areas. Rare inherited as well as de novo mutations in *trappc9* are detected in ASD probands (*10*, *11*); trappc9 mutations are actually identified as the cause of ASD in some patients (*3*, *9*). Simons Foundation Autism Research Initiative categorizes *trappc9* as a strong candidate risk gene for ASD (https://gene.sfari.org/database/human-gene/TRAPPC9#reports-tab). Trappc9 variants are also implicated in schizophrenia and attention deficit/hyperactivity disorder (*12*, *13*). How the deficiency of trappc9 impairs brain development and function remains to be defined.

Trappc9 is a subunit of TRAPP, a guanine nucleotide exchange factor (GEF) for rab proteins (*14*). Knowledge about TRAPP has been gained mainly from studies using fungal cells. Four fungal (f) TRAPP complexes are described with fTRAPP-I as the core on which additional subunits join in to form fTRAPP-II, fTRAPP-III, and fTRAPP-IV (*14*). All four fTRAPPs display GEF activities onto ypt1 (rab1) in vitro; fTRAPP-II is also a GEF for ypt31/32 (rab11) (*14*). Two metazoan (m) TRAPP complexes termed mTRAPP-II and mTRAPP-III, which are specified by trappc9/10 and trappc8/11/12/13, respectively, are proposed and play opposing roles in regulating intracellular ricin transport (*15*). Hence, mTRAPP-II and mTRAPP-III are likely to activate two different rabs so that opposing roles can be achieved. However, these rabs are not completely defined. mTRAPP-II is suggested to be a GEF for rab1 and rab18 (*16*), but its role in activating rab18 is disputed (*17*). Studies using an in vitro assay containing no biomembranes show that mTRAPP-II has no GEF activity on rab11 (*18*). The presence of biomembranes was demonstrated in later studies to be crucial for fTRAPP-II to display robust GEF activities onto ypt31/32 (*19*). Therefore, further studies are needed to determine whether mTRAPP-II is a bona fide GEF for rab11. The function of mTRAPP in mammals is largely unknown, but genetic mutations disabling several mTRAPP subunits have been linked to ID with brain malformations similar to trappc9-linked ID (*20*–*25*). The lack of genetically modified mammals deficient for mTRAPP subunit(s) restricts us from exploring pathogenic mechanisms and therapeutic strategies for these diseases.

The striatum integrates information coming from nearly the entire cerebral cortex and various subcortical brain structures to coordinate multiple aspects of cognition and contributes to numerous neuropsychiatric disorders (*26*–*30*). Most neurons in the striatum are medium spiny neurons (MSNs) and are divided into two main subtypes based on their expression of dopamine receptors and projection via the direct or indirect pathway. Striatal MSNs in the direct pathway express D1-like dopamine receptors (D1R) and promote motor activity, whereas MSNs in the indirect pathway express D2-like receptors (D2R) and inhibit motor activity. A balance between D1R and D2R MSNs is needed for normal functions of the striatum; disruption of the balance underlies cognitive and motor disturbances in diverse neuropsychiatric disorders including Parkinson's and Huntington's disease, attention deficit/hyperactivity disorder, obsessive-compulsive disorder, ASD, and schizophrenia (*26*, *27*, *30*). Volume change of the striatum is also suggested to be a pathogenic contributor of ASD and schizophrenia, as enlargement of the striatum is noted in medication-free ASD and schizophrenia (*26*, *31*).

[1]School of Pharmacy, Shanghai Jiao Tong University, 800 Dong Chuan Road, Shanghai 200240, China. [2]Department of Neurology, Massachusetts General Hospital and Harvard Medical School, Charlestown, MA 02129, USA. [3]Mucosal Immunology Laboratory, Combined Program in Pediatric Gastroenterology and Nutrition, Massachusetts General Hospital and Harvard Medical School, Charlestown, MA 02129, USA. [4]Department of Nephrology, Shanghai General Hospital, 650 Songjiang Road, Songjiang District, Shanghai 201620, China.
*Corresponding author. Email: xueyili@sjtu.edu.cn, xueyi.li@mgh.harvard.edu

In this study, we generated trappc9 null mice and examined them to determine whether they developed phenotypes resembling those discerned in patients with ID bearing trappc9 mutations. Trappc9 null mice exhibited a broad range of behavioral deficits and postnatal delay in size accrual of the brain as well as decreased volume of various brain structures relative to wild-type (WT) mice. Trappc9 null mice manifested enlargement of the striatum, in which the ratio of D1R and D2R neurons was altered. We demonstrate that behavioral deficits in trappc9 null mice can be mitigated with pharmaceutics that modulate activities of dopamine receptors. In addition, we found that abrogation of trappc9 reduced the activation of rab11 with little effect on rab1 activation. Our study not only provides a new murine model but also elicits a pathogenic mechanism and a potential treatment for trappc9-linked ID and other associated disorders.

RESULTS

Trappc9-deficient mice exhibit a wide range of behavioral deficits

To learn how the deficiency of trappc9 disrupts brain development and function, we generated a line of trappc9 null [KO (knockout)] mice (fig. S1). Consistent with the finding of failed division of spermatocytes when *Drosophila* trappc9 is inactivated (*32*), male trappc9 KO mice might be sterile because pregnancy of WT or heterozygous (HZ) females was never achieved when male trappc9 KO mice were used as breeding mates. Female trappc9 KO mice showed a decline in reproduction relative to WT female mice (fig. S1E). Trappc9 KO mice were normal in gaining body weight during the preweaning period, but gained significantly more weight than WT mice after weaning (fig. S1F). Female trappc9 KO mice appeared overweight earlier than male trappc9 KO mice (fig. S1F). The life span of trappc9 KO mice was normal (fig. S1G).

Having obtained trappc9 KO mice, we then conducted a battery of behavioral tests to examine effects of trappc9 deficiency on brain functions. Compared with WT mice, trappc9 KO mice were hypoactive and less likely to explore in open areas of an open field arena or in open arms of an elevated plus maze (Fig. 1, A and B). While trappc9 KO mice were able to recognize or memorize a familiar object or cognate (fig. S2, A and B), female trappc9 KO mice showed less interest in interacting with a novel object or an unfamiliar cognate relative to female WT animals (Fig. 1, C and D). Despite having a normal grip strength and no restriction in body movements (fig. S2, C and D), trappc9 KO mice fell off an accelerated rotarod more frequently than WT mice; performance was normalized with additional training (fig. S2E), suggesting that the poor performance of trappc9 KO mice on an accelerated rotarod arises from a deficit in motor skill learning and memory instead of impaired motor coordination. Trappc9 null mice were similar to WT mice in vision and swimming ability (fig. S2F) but were significantly slower to learn to find the submerged platform than WT mice in acquisition trials (Fig. 1E, acquisition trial). When the hidden platform was removed (probe trial), trappc9 KO mice crossed the original locus of the hidden platform less frequently and swam for significantly less time in the target quadrant than WT animals, although trappc9 KO mice swam as fast as in the first trial of the test (Fig. 1E, probe trial). Male trappc9 KO mice were comparable to WT mice in other behavioral tests (Fig. 1, B and C, and fig. S2), but were very aggressive after behavioral tests (data not shown). These observations suggest that trappc9 deficiency in mice causes defects in multiple aspects of brain function including learning and memory.

Trappc9 deficiency in mice causes brain malformations

As trappc9 KO mice display a broad range of behavioral deficits reflecting global delay of intellectual development seen in patients with trappc9 mutations, we wanted to know if trappc9 KO mice had brain structural malformations characteristic of patients with ID. Consistent with the observation of postnatal microcephaly in patients with trappc9 mutations, the brain size of trappc9 KO mice was normal at birth, but became significantly smaller than WT at postnatal day 7 (p7) and all later ages examined (Fig. 2A). Other organs of trappc9 KO mice were of similar size or enlarged relative to those of WT mice (fig. S3).

The trappc9 protein was detected throughout the brain and present in neurons and astrocytes (fig. S4). Trappc9 KO mice expressed comparable levels of neuronal nuclear protein (NeuN) to WT mice, but had a significant elevation and decline in levels of glial fibrillary acidic protein (GFAP) and oligodendrocyte lineage transcription factor Oligo-2, respectively (fig. S5, A and B). Counting of NeuN-positive cells in brain sections with stereological methods revealed similar densities of neurons in the brain of trappc9 KO and WT mice (fig. S5, C and D), suggesting that behavioral deficits observed in trappc9 KO mice do not arise from loss of neurons in the brain.

To determine whether trappc9 KO mice had atrophy of brain structures similar to patients with ID, cross-sectional areas of brain structures were measured in sagittal brain sections of WT and trappc9 KO mice. The corpus callosum of trappc9 KO mice was significantly thinner than that of WT mice (Fig. 2B). Besides, trappc9 KO mice manifested a significant volume decline in the hippocampus, the cerebellum, and the pons and medulla oblongata (Fig. 2B). These data suggest that atrophy of brain structures in trappc9 KO mice resembles brain pathologies in patients with ID with trappc9 mutations.

Trappc9 deficiency disturbs the ratio of dopamine D1 and D2 neurons in the brain

Contrary to whole brain shrinkage and atrophy of various brain structures described above, the striatum of trappc9 KO mice was enlarged (Fig. 2B). Considering that striatal enlargement and trappc9 variants are associated with ASD and schizophrenia (*26*, *31*), we reasoned that striatal enlargement might be a pivotal contributor to brain dysfunction in trappc9 null mice. MSNs constitute 90 to 95% of total neurons in the striatum and are enriched in adenosine 3′5′-monophosphate-regulated phospho-protein molecular weight 32 kDa (DARPP32) (*33*). We wondered whether trappc9 deficiency influenced the development of DARPP32-positive neurons. Consistent with striatal enlargement, levels of DARPP32 in brain lysates of trappc9 KO mice were significantly elevated relative to those in brain lysates of WT mice (Fig. 2C). However, the density of DARPP32-positive neurons in the striatum of WT and trappc9 KO mice was comparable (Fig. 2C), suggesting that the content of neurons and not neuronal density in the striatum increases proportionally to the volume change.

Striatal MSNs are classically divided into D1R and D2R subpopulations. Imbalance between these two populations of neurons is associated with various disease conditions including ASD and schizophrenia (*26*, *27*, *30*). To determine whether the balance between D1R and D2R neurons was altered in the brain of trappc9 KO mice, we compared expression levels of D1R and D2R proteins in

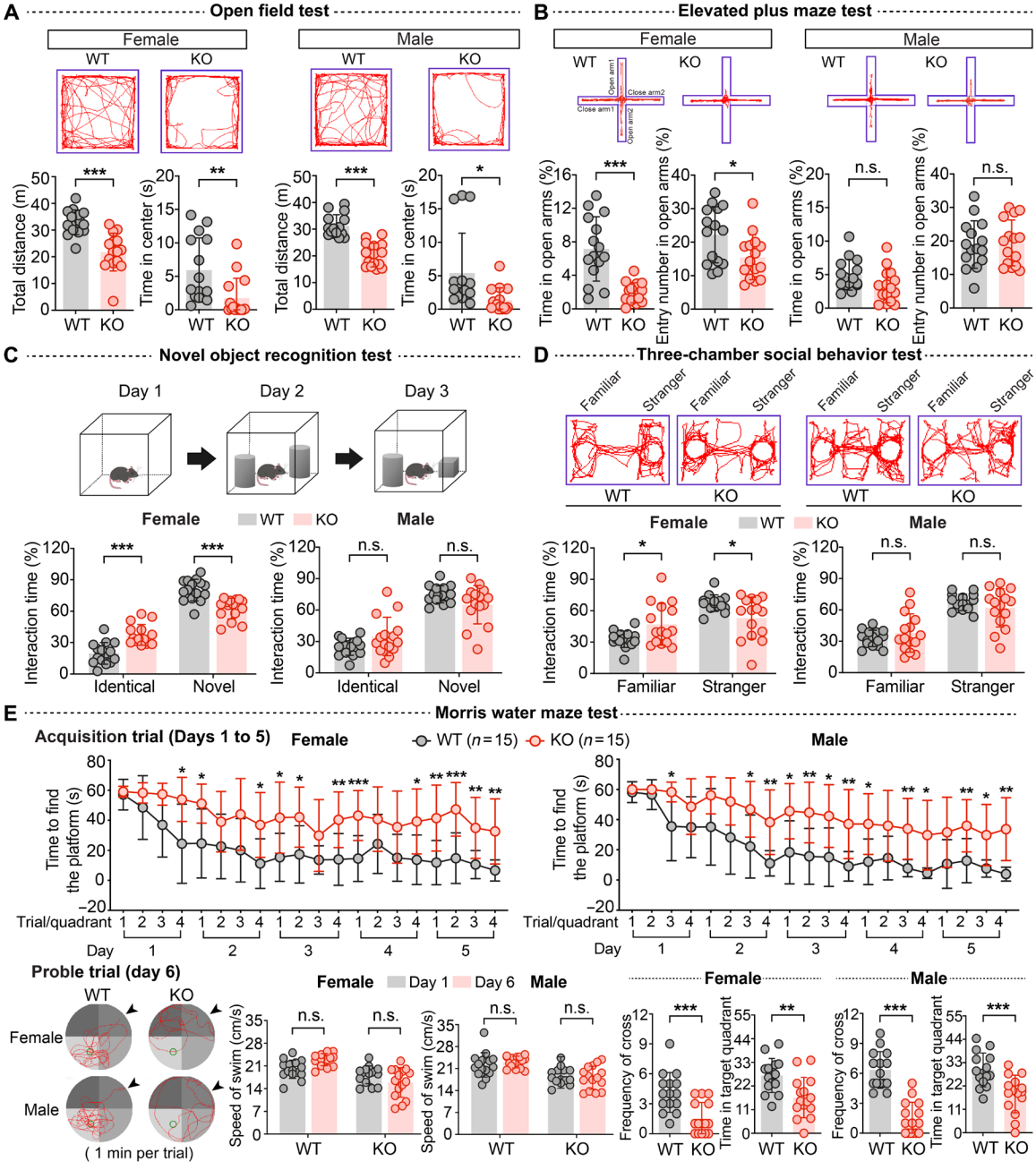

Fig. 1. Abrogation of trappc9 causes a wide range of behavioral deficits. Trappc9 KO and WT mice from 8 weeks of age ($n = 30$ per genotype) were subjected to behavioral tests. (**A**) Trappc9 KO mice displayed a significant decrease in both total distance traversed in the open arena and time spent in central areas of the arena. (**B**) Trappc9 KO female mice entered less frequently into open arms and spent less time in open arms relative to WT mice. Trappc9 KO female mice did not show a preference to a novel object (**C**) or to a stranger mouse (**D**) as did WT mice. Compared with WT mice, trappc9 KO mice spent a longer time to locate the submerged platform [(**E**) acquisition trial, two-way repeated-measures analysis of variance (ANOVA), female: $F_{19,532} = 1.621$, $P = 0.047$; male: $F_{19,532} = 1.791$, $P = 0.021$] and, in the probe trial, swam for significantly less time in the target quadrant and crossed the target locus less frequently than WT mice despite having a comparable swimming speed relative to WT mice or to the first day of the trial. Representative trajectories are shown above the scatterplots with bar in (A), (B), and (D) or left to the plots in (E, probe trial). Schematic diagrams shown above the scatterplots with bar in (C) are testing procedures. Arrowheads beside trajectory graphs in (E, probe trial) point to the locus where tested animals were placed. In all scatterplots with bar, each symbol represents one animal. Data are means ± SD. Statistical significance in (A) to (D) and (E, probe trial) was determined by two-tailed unpaired Student's *t* test, except two-tailed paired Student's *t* test being used for comparison of swimming speed between days 1 and 6 in (E, probe trial). All graphs, $^*P < 0.05$; $^{**}P < 0.01$; $^{***}P < 0.001$; n.s., no significance.

the brain of trappc9 KO and WT mice. Our results showed that levels of D1R were elevated whereas levels of D2R were diminished in brain lysates of trappc9 KO mice relative to their levels in WT mouse brain lysates (Fig. 2, D and E), a sign of disruption of the balance between D1R and D2R neurons. We then conducted immunohistochemistry studies to examine whether the content of D1R and

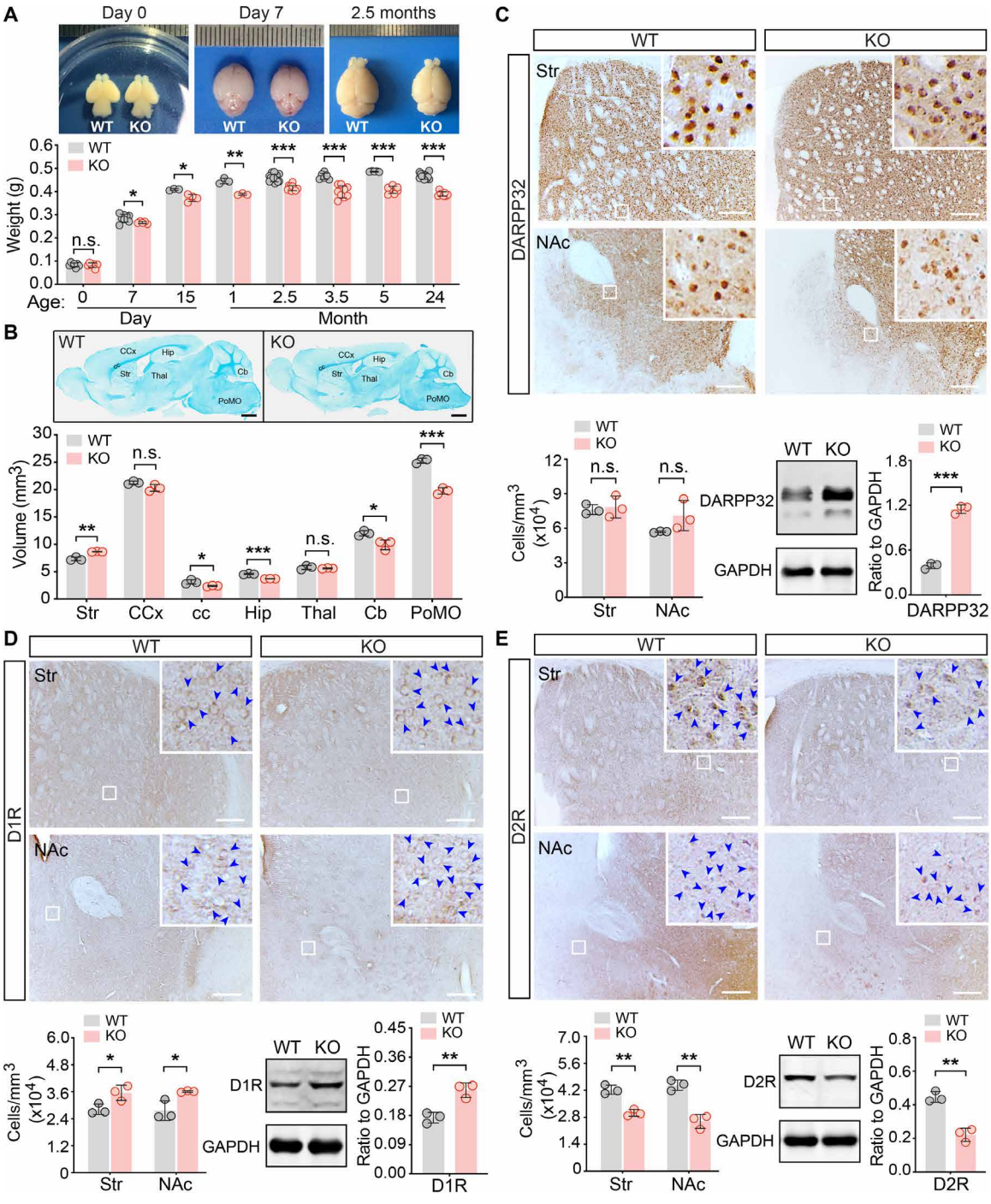

Fig. 2. Trappc9 deficiency alters the proportion of dopamine receptive neurons in the striatum and nucleus accumbens. (**A**) Postnatal delay in growth of the brain in trappc9 KO mice. Brains with scales shown above the bar graph are from p0, p7, and 10-week-old trappc9 KO mice and their corresponding WT littermates. Photo credit: Yuting Ke, Muhammad Usman and Pinky Sultana, Shanghai Jiao Tong University. (**B**) Luxol fast blue–stained brain sections used for measuring volumes of brain structures. Quantitative data from three consecutive sections per mouse are graphed ($n = 3$ mice per genotype). Scale bars, 1 mm. Str, striatum; CCx, cerebral cortex; cc, corpus callosum; Hip, hippocampus; Thal, thalamus; Cb, cerebellum; PoMO, pons and medulla oblongata. (**C**) Brain sections for stereology quantification of DARPP32-positive cells in the striatum (Str) and nucleus accumbens (NAc). Insets are the enlarged boxed regions. Panels below brain sections: Left bar graph shows stereology quantification data from three consecutive sections of each mouse ($n = 3$ mice per genotype), middle panel shows a blot analysis of DARPP32 in brain lysates of WT and trappc9 KO mice, and right bar graph summarizes densitometry data from three mice of each genotype. Glyceraldehyde-3-phosphate dehydrogenase (GAPDH) is a loading control. Stereology quantification of D1R-positive (**D**) and D2R-positive (**E**) neurons in the Str and NAc, and Western blot analysis followed by densitometry quantification of levels of D1R (D) and D2R (E) in brain lysates are conducted as in (C). Brain sections and brain lysates used for analyses in (C) to (E) are from the same mice. Arrowheads in insets in (D) and (E) indicate neurons positive for D1R and D2R, respectively. Scale bars in (C) to (E), 300 μm. Data are means ± SD. In all scatterplots with bar, each symbol represents one animal. Two-tailed Student's *t* test: $^{*}P < 0.05$; $^{**}P < 0.01$; $^{***}P < 0.001$.

D2R containing neurons was changed in the brain of trappc9 KO mice. Neuronal counts using stereology methods revealed that densities of D1R- and D2R-positive neurons in the striatum and nucleus accumbens of trappc9 KO mice were increased and decreased, respectively, when compared with their corresponding densities in WT mice (Fig. 2, D and E). Collectively, these data indicate that trappc9 deficiency alters the proportion of dopamine D1R and D2R neurons in the striatum and nucleus accumbens.

There are also dense networks of dopaminergic innervation in the hippocampus and the prefrontal cortex, where the dopamine signaling system modulates novelty processing, decision-making, attention, and spatial learning and memory (*34*, *35*). Hence, we asked whether the balance of dopamine receptive neurons in these brain regions of trappc9 null mice was altered as well. We harvested brain tissues from a group of 2- to 3-month-old WT and trappc9 KO mice for side-by-side comparison of expression levels of D1R and D2R in the hippocampus, striatum, and cerebral cortex. We observed similar changes in expression levels of D1R and D2R in the striatum of a different cohort of trappc9 KO mice to those shown above (fig. S6, A to C, and Fig. 2). While levels of DARPP32 in the cerebral cortex of trappc9 KO mice were significantly increased relative to those in WT mice (fig. S6A), there was no significant difference in levels of D1R or D2R in cerebral cortices between trappc9 KO and WT mice (fig. S6, B and C), suggesting that the balance between D1R and D2R neurons in the cerebral cortex of trappc9 KO mice is still maintained. Levels of DARPP32, D1R, and D2R were all significantly reduced in the hippocampus of trappc9 KO mice compared with their levels in WT mice (fig. S6, A to C). Contrary to an increase in the striatum, the ratio of D1R to D2R neurons in the hippocampus of trappc9 KO mice was decreased (n = 3 WT and 3 KO mice; means ± SD; WT versus KO: 0.232 ± 0.0222 versus 0.122 ± 0.0155; two-tailed Student's t test: $P < 0.01$).

We then asked when the ratio of dopamine-receptive neurons in the brain of trappc9 null mice was changed. We collected brain tissues of mice aged at p0 (day of birth), p7, p15, and p30 for examining levels of D1R and D2R. Similar levels of DARPP32 in the brain of trappc9 KO and WT mice occurred at all ages examined (fig. S6D). However, a change in levels of D1R and D2R neurons was detected in the brain of trappc9 null mice at p30, but not in mice p15 or younger (fig. S6, E and F), suggesting that imbalance between D1R and D2R neurons takes place at a stage when exploratory activities of mice vastly increase. Our observation of similar levels of DARPP32 in the brain of WT and trappc9 KO mice at p30 or younger suggests that enlargement of the striatum in 12-week-old trappc9 KO mice may be a compensatory effect for the dysfunction or decreased density of D2R neurons in the striatum.

Pharmacological modulation of dopamine receptors improves behavioral performances of trappc9 null mice

In view of the observations above, we speculated that behavioral defects in trappc9 KO mice might result from functional imbalance between D1R and D2R neurons. If so, pharmacological manipulation of D1R and/or D2R should improve performances of trappc9 KO mice on behavioral tasks. We treated trappc9 KO mice with a bolus of D1R antagonist SCH23390 or D2R agonist quinpirole alone and evaluated drug effects with the open field test. Motor inhibition as indicated by animal immobility occurred as expected a few minutes after drug administration (data not shown). While neither SCH23390 nor quinpirole could increase the travel distance, each drug alone triggered a gradual increase in the time spent in central areas of the open field (fig. S7).

The beneficial effects of SCH23390 or quinpirole on motivating trappc9 KO mice to explore in central areas of the open field led us to speculate that a combination of SCH23390 and quinpirole might elicit greater beneficial effects than each of them alone. We continued to employ the open field test to evaluate drug effects at different times following drug administration (fig. S8A). Upon treatment with both SCH23390 and quinpirole, exploratory activities of trappc9 KO mice temporarily declined and were recovered back to levels of vehicle-treated trappc9 KO mice 3 hours after administrating both drugs (fig. S8B). Notably, treatment with both compounds for 24 hours elevated exploratory activities in both travel distance and time spent in central areas of trappc9 KO mice to levels of WT mice (Fig. 3A). The beneficial effects waned 48 hours after drugs were administrated (fig. S8B).

We next determined whether a combination of SCH23390 and quinpirole could improve performances of trappc9 KO mice on other cognitive tasks. Treatment with both compounds did not change the ability of trappc9 KO mice to randomly explore two identical objects or empty chambers, nor did it affect their preference to interact with a familiar cognate to an object (fig. S8C, Fig. 3B). However, administration of a single dose of each of SCH23390 and quinpirole significantly escalated the interest of trappc9 KO mice in interacting with a novel object and with an unfamiliar cognate (Fig. 3, B and C). In the Morris water maze test, SCH23390 and quinpirole treatment significantly accelerated trappc9 KO mice to find the submerged platform in all acquisition trials and elevated the swimming speed of trappc9 KO mice as well as the frequency that trappc9 KO mice crossed the original locus of the hidden platform to levels of WT mice in the probe trial (Fig. 3D). Collectively, these data support the idea that disrupted balance between D1R and D2R neurons underscores behavioral deficits in trappc9 KO mice and suggest that drugs acting on dopamine receptors may be beneficial for patients with ID who lose the expression of the trappc9 protein.

Trappc9 loss causes astrogliosis in the hippocampus and the corpus callosum

The above biochemical studies revealed that there was a significant increase in levels of GFAP in the brain of trappc9 KO mice (fig. S5A), a sign of astrogliosis. To unveil brain area(s) in which astrogliosis took place, we processed a series of coronal brain sections of WT and trappc9 KO mice for double immunofluorescence labeling with antibodies for trappc9 and GFAP (Fig. 4A). Quantification of fluorescence intensities of GFAP immunoreactive signals in different brain areas showed that astrogliosis was present in the corpus callosum and the hippocampus of trappc9 null mice (Fig. 4B). Coincidentally, these two structures are atrophic in trappc9 KO mice. As the hippocampus plays a crucial role in spatial learning and memory, which is impaired in trappc9 KO mice, we carried out further analysis and found that astrogliosis culminated at the radiatum and lacunosum moleculare layers of the hippocampus and the polymorph layer of the dentate gyrus (Fig. 4C). Astrogliosis is a defensive reaction of astrocytes to promote recovery of the central nervous system from harmful stimuli, but persistent astrogliosis can be detrimental and is frequently seen in a plethora of neuropsychiatric diseases (*36*). However, it is not clear whether astrogliosis in these brain regions occurs normally in response to harmful stimuli or is a culprit of pathological changes in the brain of trappc9 null mice.

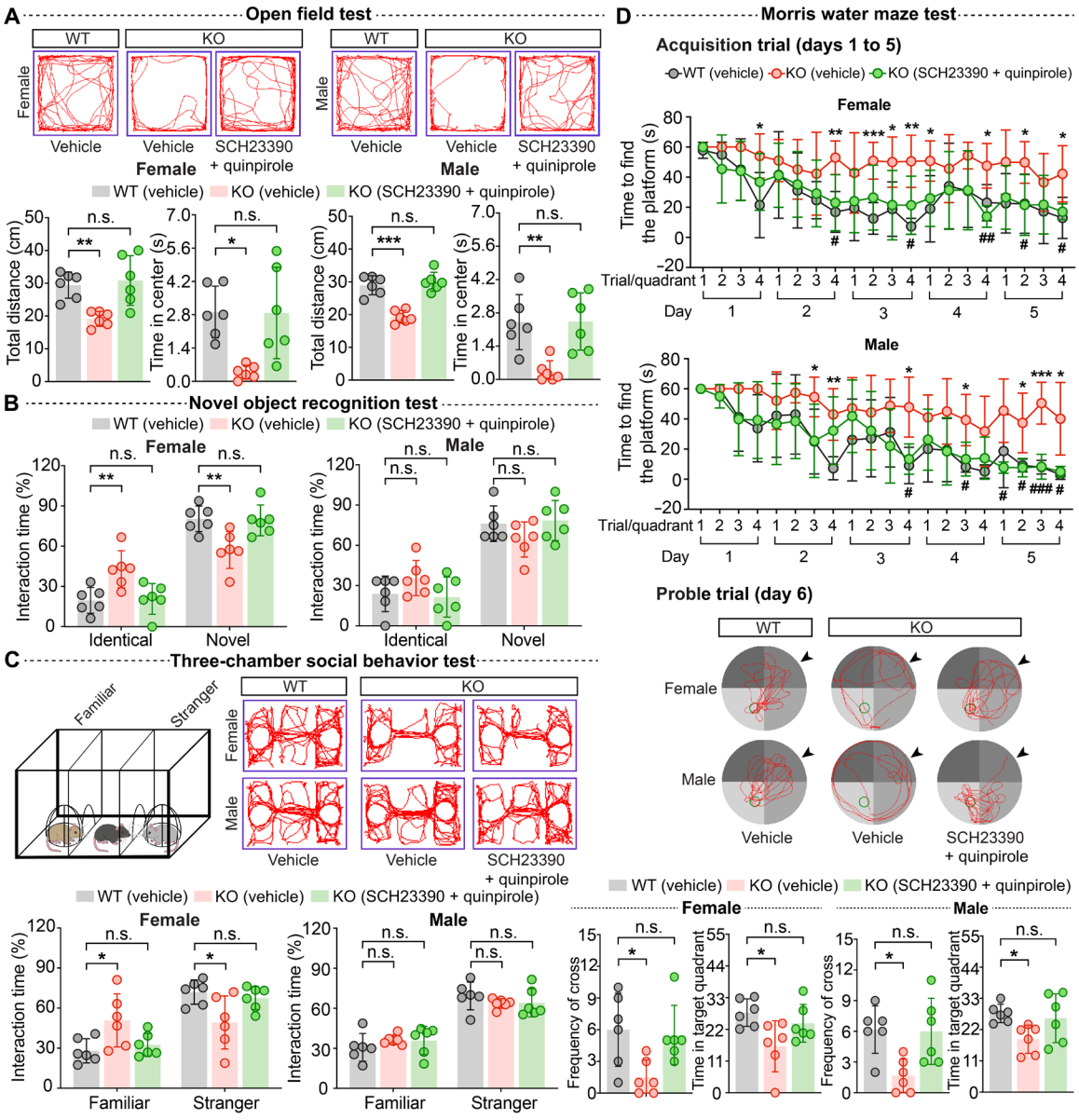

Fig. 3. Pharmacological manipulation of dopamine receptors in trappc9 null mice attenuates behavioral deficits. A cohort of trappc9 KO mice ($n = 12$ per gender) from 8 weeks of age are given either a dose of SCH23390 and quinpirole or the same volume of physiological saline (vehicle) 24 hours before evaluating spontaneous exploratory activities in an open arena (**A**), sociability with a novel object (**B**) or with a strange cognate (**C**), and spatial learning and memory (**D**). Age- and gender-matched WT mice ($n = 6$ per gender) were evaluated as normal controls. Treatment with SCH23390 and quinpirole significantly improves trappc9 KO mice to explore in open areas [(A) distance, female: $F_{2,15} = 9.284$, $P < 0.01$; male: $F_{2,15} = 30.67$, $P < 0.0001$; time in central areas, female: $F_{2,15} = 7.606$, $P < 0.01$; male: $F_{2,15} = 8.788$, $P < 0.01$], to interact with a novel object [(B) female: $F_{2,15} = 7.466$, $P < 0.01$; male: $F_{2,15} = 1.827$, $P = 0.195$] or with a stranger mouse [(C) female: $F_{2,15} = 4.732$, $P < 0.05$; male: $F_{2,15} = 0.762$, $P = 0.484$], to learn to find the submerged platform [(D) acquisition trials, two-way repeated-measures ANOVA, female: $F_{38,285} = 0.971$, $P = 0.522$; male: $F_{38,285} = 1.169$, $P = 0.238$], and to recall the locus where the hidden platform was originally placed [(D) probe trial, crossing frequency, female: $F_{2,15} = 4.845$, $P = 0.024$; male: $F_{2,15} = 6.356$, $P = 0.01$; time in target quadrant, female: $F_{2,15} = 4.426$, $P = 0.031$; male: $F_{2,15} = 3.869$, $P = 0.044$]. Representative trajectories of a mouse from each group are shown on scatterplots with bar in (A), (C), and (D, probe trial). Data are means ± SD. In all scatterplots with bar, each symbol represents a mouse. Unless indicated, comparisons are done with one-way ANOVA followed by Tukey's multiple comparison tests. WT versus vehicle-treated KO, $^{*}P < 0.05$; $^{**}P < 0.01$; $^{***}P < 0.001$; vehicle versus drug-treated KO, #$P < 0.05$; ##$P < 0.01$; ###$P < 0.001$.

Loss of trappc9 disturbs the function of rab11

Having unveiled macrostructures and cell populations likely responsible for impaired brain functions in trappc9 KO mice, we then made efforts to elucidate molecular pathway(s) affected by the deficiency of trappc9. As skin fibroblasts of patients with trappc9 mutations present a sign of defective activation of nuclear factor κB (NF-κB) (*7*), we looked for evidence of deficient activation of NF-κB in the brain of trappc9 KO mice. We analyzed levels of NF-κB components and related posttranslational modifications on them. Our results showed no evidence of deficient activation of NF-κB in the brain of trappc9 KO mice (fig. S9). Hence, NF-κB is unlikely to be a main contributor to the impairment of brain development and function in trappc9 KO mice.

In fungal cells, trappc9 (trs120) interacts with trappc10 (trs130) to switch the GEF activity of fTRAPP toward ypt31/rab11 from

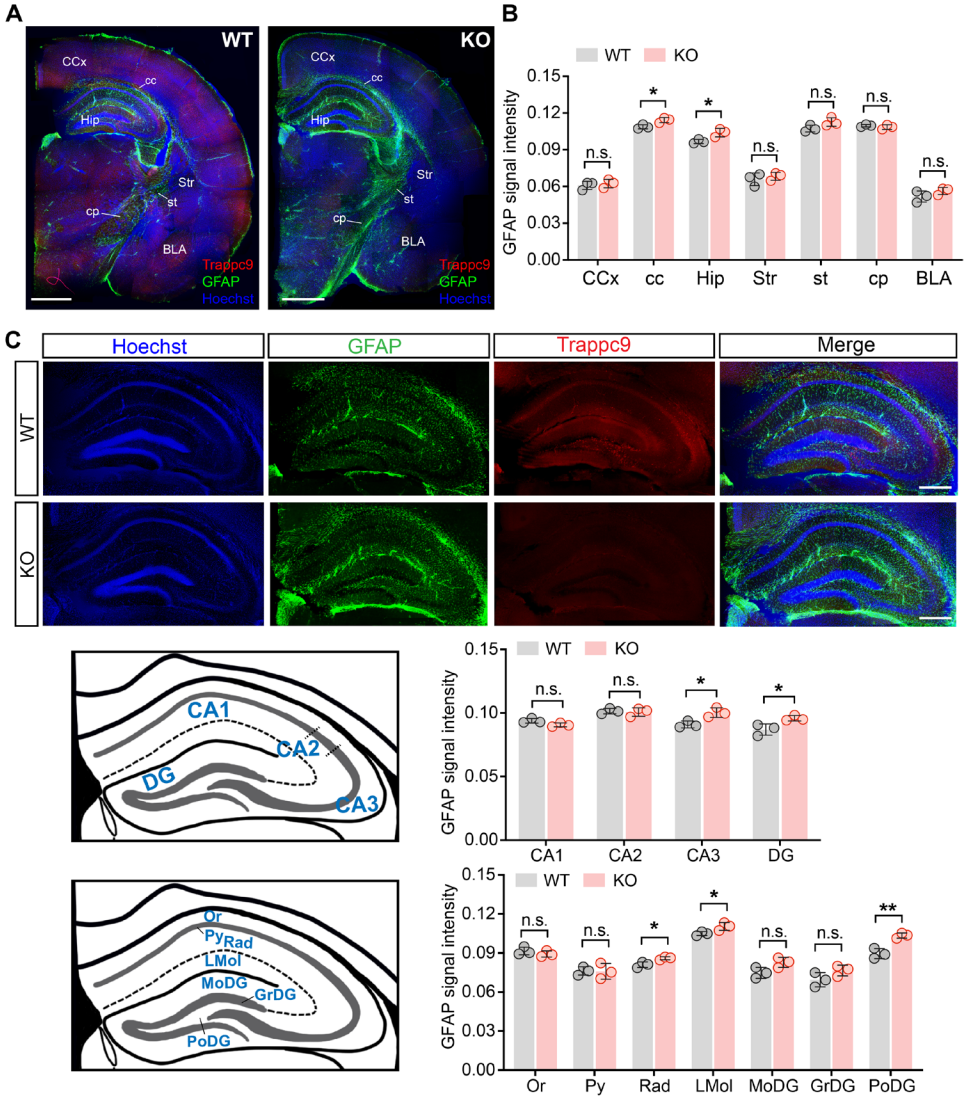

Fig. 4. Astrogliosis in the brain of trappc9-deficient miceABC. (**A**) Immunofluorescence labeling of brain sections with antibodies for GFAP (green) and trappc9 (red) to unveil the brain region(s) where astrogliosis occurs. Cells are identified by staining nuclei with Hoechst 34580 (blue). Coronal sections are cut from half brains of WT and trappc9 KO mice. Images of different channels were collected separately from different but overlapping areas of each brain section so as to image the whole brain section and merged using Photoshop. Individual merged images of different brain areas were realigned into one image using Adobe Illustrator. Shown are representative realigned images of a brain section for each genotype. Scale bars, 1 mm. (**B**) Densitometry quantification of GFAP signals in different brain regions using realigned images from three consecutive brain sections of each of three mice per genotype reveals astrogliosis in the corpus callosum and the hippocampus of trappc9 KO mice. In (A) and (B), CCx, cerebral cortex; cc, corpus callosum; Hip, hippocampus; Str, striatum; st, stria terminalis; cp, cerebral peduncle; BLA, basolateral amygdala. (**C**) Representative images of WT and trappc9 KO hippocampi used for densitometry quantification of GFAP signals in different areas and layers. Scale bars, 400 μm. The diagrams illustrate the boundaries for defining the areas and layers of the hippocampus. Bar graphs shown left to the diagrams are quantitative data of GFAP signals in different areas and layers of the hippocampus from three consecutive sections of each of three mice per genotype. CA1 to CA3, hippocampal cornu ammonis 1 to 3; DG, dentate gyrus; Or, oriens layer; Py, pyramidal cell layer; Rad, radiatum layer; LMol, lacunosum moleculare layer; MoDG, molecular layer of DG; GrDG, granule cell layer of DG; PoDG, polymorph layer of DG. Data are means ± SD. Statistical significance is determined by two-tailed Student's *t* test: $^{*}P < 0.05$; $^{**}P < 0.01$.

ypt1/rab1 (*14*, *19*). In studies to search for a GEF for rab11 in mammals, we identified trappc9 and trappc10 from proteins precipitated by dominant negative rab11 (dNrab11) and verified that besides trappc9/10, trappc4, one of the four subunits forming a core that endows GEF activities to TRAPP (*14*), was also associated with dNrab11 (Fig. 5, A and B). Under the same conditions, trappc11, which specifies mTRAPP-III (*15*), was not precipitated by dNrab11 (Fig. 5B). These data demonstrate that mTRAPP-II physically interacts with inactive rab11 and thus meets the prerequisite to act as a rab11GEF. mTRAPP-II enriched with trappc9 from human embryonic kidney 293T cells released [^{3}H]GDP from rab11 and rab1, but not rab5 (Fig. 5, C and D), indicating that mTRAPP-II is a bona fide GEF for rab11 in mammals.

Next, we determined whether the activation of rab1 and rab11 was affected in the brain of trappc9 KO mice. Ablation of trappc9 markedly depleted trappc10 but had little effect on expression levels of trappc11 (fig. S10, A and B), suggesting that mTRAPP-III is assembled normally and hence unlikely to contribute to changes of

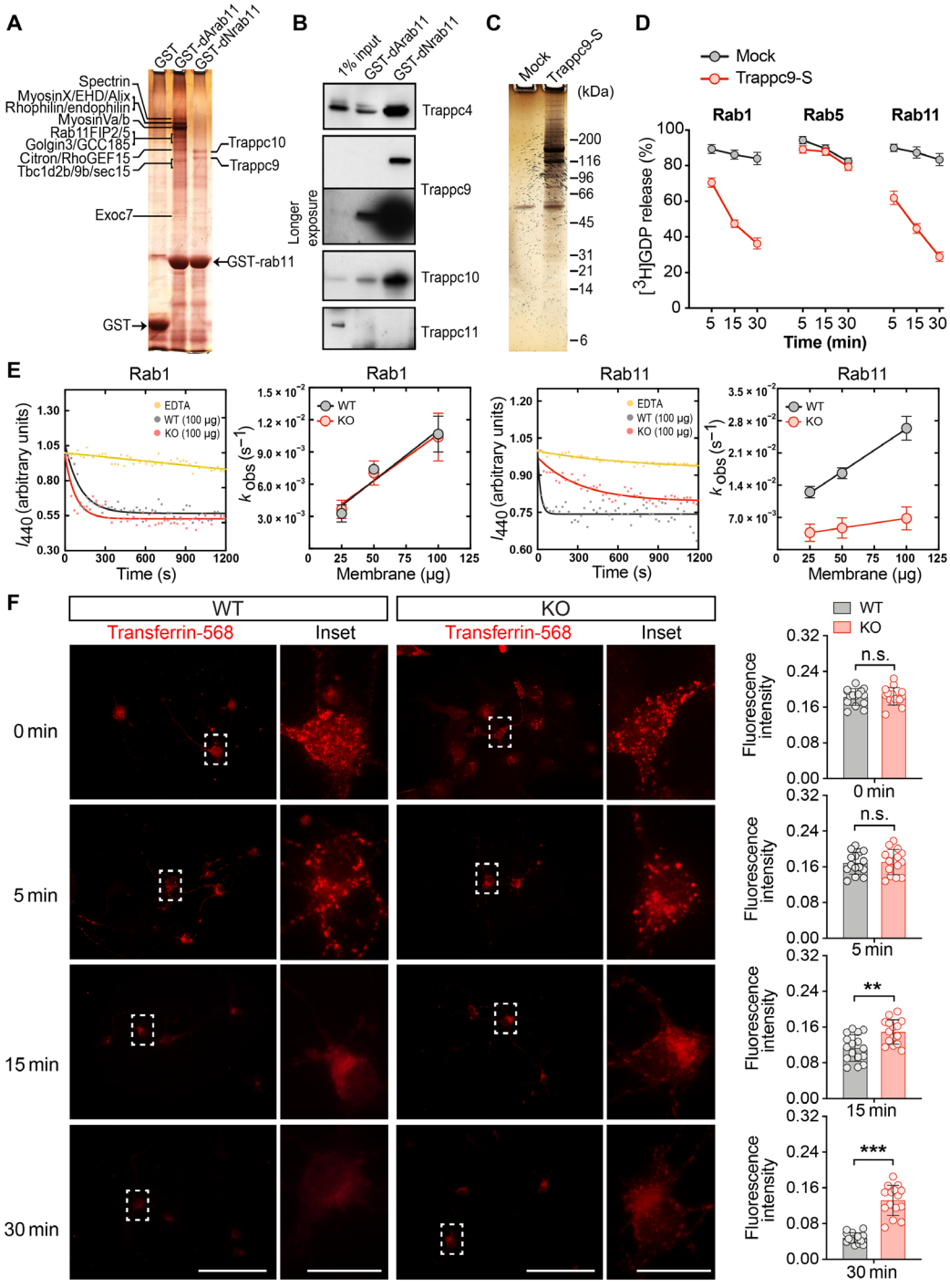

Fig. 5. Depletion of trappc9 compromises the function of rab11. (**A**) SDS–polyacrylamide gel electrophoresis (SDS-PAGE) followed by silver stain detecting proteins precipitated by rab11 mutants (dNrab11 and dArab11). Shown beside the gel graphs are proteins identified by mass spectrometry analysis of gel slices containing the corresponding silver-stained protein bands. (**B**) Western blot analysis confirms that besides trappc9 and trappc10, trappc4 but not trappc11 is associated with dNrab11. (**C**) Representative graph of silver-stained gels showing proteins enriched with S-protein resins from cellular membranes of 293T cells expressing S-tagged trappc9 (Trappc9-S) or GFP alone (mock) and used for [^{3}H]GDP release assays (D). Plots in (**D**) show that proteins enriched with S-protein resins from cellular membranes of 293T cells expressing Trappc9-S accelerated release of [^{3}H]GDP from rab1 and rab11 but not rab5. S-protein resins incubated with cellular membranes of 293T cells expressing GFP alone are used as mock GEF controls. Data are means ± SD of three independent experiments. (**E**) Kinetics of fluorescent GDP release from rab1 and rab11 in the presence or absence of 10 mM EDTA (yellow) or 25, 50, or 100 µg of cellular membranes prepared from brain tissues of WT (gray) or trappc9 KO (red) mice ($n = 3$ animals per genotype). Fluorescent signals of corresponding amounts of brain membranes are also measured and used as background signals. Mean ± SD of k_{obs} is calculated from data obtained from three different mice per genotype. (**F**) Representative images of primary neurons of WT and trappc9 KO mice after synchronized uptake of Alexa 568–transferrin for indicated times. Scale bars, 100 µm; 20 µm for insets. Means ± SD of signal intensities of intracellular Alexa 568–transferrin fluorescence are graphed and shown to the right of images of neurons incubated for the corresponding time ($n = 15$ neurons per genotype in each condition, two-tailed Student's t test: $^{**}P < 0.01$; $^{***}P < 0.001$).

GEF activity in trappc9 KO mice. To our surprise, depletion of trappc9 did not alter rab1GEF activity in brain membranes, yet significantly diminished GEF activities on rab11 (Fig. 5E), indicating that trappc9/10-specified mTRAPP-II selectively activates rab11 in vivo, whereas trappc11-defined mTRAPP-III activates rab1. These data also suggest that trappc9 deficiency may cause improper function of rab11. In agreement with this idea, levels of rab11 were up-regulated in the brain of trappc9 KO mice; under the same conditions, there was no significant change in levels of other endosome-associated rabs or rab18 (fig. S10, C and D), which is suggested to be a substrate of mTRAPP-II (*16*). REI-1/SH3BP5 acts as a GEF for rab11 in nematodes and flies and is highly conserved across species including human (*17*, *37*). We examined and found no change in levels of SH3BP5 in the brain of trappc9 KO mice (fig. S10, A and B). Hence, SH3BP5 is likely to be a main source of rab11GEF activities in brain membranes of trappc9 KO mice.

To determine whether trappc9 deficiency altered the function of rab11, we first compared the subcellular distribution of rab11 in WT and trappc9 KO mouse embryonic fibroblasts (MEFs). Compared with a diffuse pattern of rab11 signals in WT MEFs, rab11 immunoreactive signals in trappc9 KO MEFs were more concentrated at juxtanuclear areas (fig. S10E). This distribution pattern of rab11 in trappc9 KO MEFs resembles that of disease-causing rab11 mutants (*38*). We then used primary neurons cultured from WT and trappc9 KO mouse embryos to examine transferrin receptor recycling, a process widely used for measuring the function of rab11 (*39*). Consistent with a compromised function of rab11, transferrin receptor recycling was significantly impeded in trappc9 KO neurons (Fig. 5F). The morphology of the Golgi apparatus, which relies on normal function of rab1, and the distribution pattern of rab1 were comparable in WT and trappc9 KO MEFs (fig. S10E). Together with the above GEF results, we conclude that trappc9 deficiency specifically disturbs rab11 and does not influence the function of rab1.

Trappc9 deficiency diminishes dopamine D2 receptor on neuronal surfaces

Our data showed imbalance of dopamine receptive neurons and rab11 dysfunction in trappc9 KO mice. Next, we asked whether rab11 dysfunction caused the imbalance of dopamine receptive neurons in the brain of trappc9 null mice. After endocytosis, D1R is routed to cell surfaces via the retromer-dependent retrograde transport, whereas D2R undergoes rab4-dependent (constitutive) and rab11-dependent (ligand-stimulated) recycling (*40*, *41*). These retrieval pathways are interdependent; for example, enhancement of retromer-dependent retrograde transport occurs when endocytosed proteins accumulate at endosomes (*42*). Therefore, rab11 dysfunction in the brain of trappc9 KO mice is likely to compromise D2R and concurrently augment D1R recycling. To test this possibility, we labeled D1R and D2R in brain sections, which were processed with detergents omitted in all solutions to allow the integrity of the plasma membrane to be maintained so that only those D1R and D2R molecules on and close to cell surfaces were labeled. Under these experimental conditions, we observed a significant decrease in intensities of D2R and a significant increase in intensities of D1R in brain sections of trappc9 KO mice relative to their corresponding intensities in brain sections of WT mice (Fig. 6). These data are consistent with the findings that D1R and D2R recycle to cell surfaces through different routes and suggest that rab11 dysfunction in trappc9 null mice differentially influences the expression of D1R and D2R on neuronal surfaces. Persistent defect in recycling of endocytosed plasma membranes, in other words, persistent accumulation of endocytosed plasma membranes in endosomal compartments, would conceivably cause loss of plasma membranes on the cell surface, thereby reducing the cell size. In agreement with this idea, cross-sectional areas of both D1R and D2R neurons significantly declined in brain sections of trappc9 KO mice compared to those in WT mice (Fig. 6). These data suggest that rab11 dysfunction also affects D1R neurons.

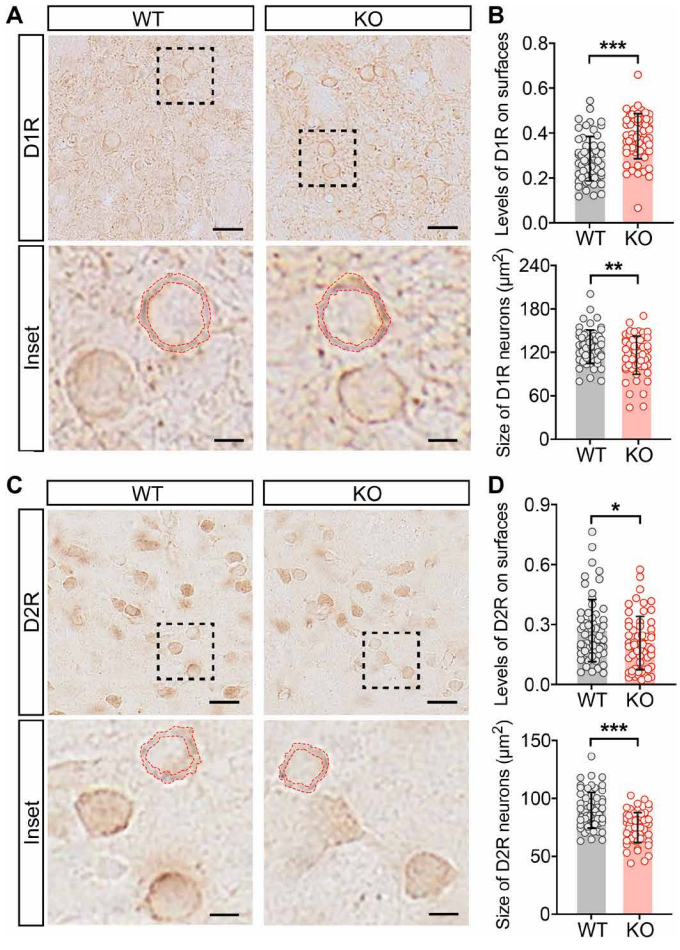

Fig. 6. Trappc9 deficiency differentially alters the expression of D1R and D2R on the surface of striatal neurons. A series of three consecutive coronal brain sections cut through the striatum of three WT and three age- and gender-matched trappc9 KO mice were processed for labeling with antibodies for D1R or D2R. The age of mice was 2 to 3 months. Detergents were omitted in all solutions to ensure the integrity of the plasma membrane. Images captured from brain sections from the same pair of WT and trappc9 KO mice show striatal neurons labeled with antibodies for D1R (**A**) or D2R (**C**). Insets in both (A) and (C) highlight typical cells chosen for measuring surface levels (top) of D1R (**B**) and D2R (**D**) as well as the size (bottom) of D1R (B) and D2R (D) neurons. Examples of analyzed neurons with two red contours in insets of (A) and (C) indicating the plasma membrane that was used for determining levels of D1R and D2R on the surface of a given neuron. Cross-sectional areas of the outer red contour were used for calculating the cell size based on the actual resolution of the original images. Images used for measurements were taken under three randomly chosen visual fields of each brain section of three WT and three trappc9 KO mice with the same settings. Three sections for each animal were analyzed. Scale bars, 20 μm; 5 μm for insets. Data are means ± SD. Statistical significance was determined by two-tailed unpaired Student's *t* test: $^{*}P < 0.05$; $^{**}P < 0.01$; $^{***}P < 0.001$.

DISCUSSION

We report three novel findings. First, we provide a new murine model of human ID. We generated a line of trappc9-deficient mice, which developed a broad range of behavioral deficits and exhibited brain structural malformations resembling those discerned in intellectually disabled patients with trappc9 mutations. Second, we elicit a potential treatment for trappc9-linked ID and other associated disorders. We found that the balance between dopamine receptive neurons was disrupted in the brain of trappc9 null mice and demonstrated that cognitive performances of trappc9 null mice were raised to levels of WT mice with pharmaceutics acting on dopamine receptors. Last, our study establishes mTRAPP-II to be a GEF specific for rab11 in mammals.

We noticed an inconsistency regarding the GEF activity on rab1 in trappc9-enriched mTRAPP-II and trappc9-void mouse brain membranes. Such discrepancy has been observed in previous studies on fTRAPP-II (*17*, *19*), although the essential function of fTRAPP-II is stated to activate ypt31/32 (*19*). In in vitro reactions, metazoan or fungal TRAPP-II, either in vitro assembled using individual subunits or enriched from cell lysates, may undergo multiple disassembly-reassembly cycles. In other words, in in vitro reactions, TRAPP-II is actually a mixture of intact TRAPP-II, which acts specifically on ypt31/32/rab11, and fragmented TRAPP complexes, which have GEF activities only onto ypt1/rab1, thus displaying apparent GEF activities toward both ypt1/rab1 and ypt31/32/rab11. Our data showing that trappc9 deficiency reduces GEF activities in brain membranes for activating rab11 but not rab1 help to resolve the perplexity on the specificity of m/fTRAPP-II in activating its substrate rab (*17*).

In addition to our results, there is support from other studies that improper function of rab11 mediates the detrimental effects of trappc9 deficiency on brain development and function. Genetic mutations in *rab11* cause severe ID with brain structural changes similar to those in patients with ID bearing trappc9 mutations (*38*). In response to a constant decrease in generating active rab11, trappc9 null mice might develop compensatory effects by raising expression levels of rab11. Rab11 is well known for its role in endocytic recycling of receptors, transporters, and other critical plasma membrane constituents, thereby sustaining functional plasticity of cells. A myriad of proteins critical for brain functions have been identified as rab11 regulated trafficking cargoes (*39*), although rab11-dependent endocytic recycling in the central nervous system has been an underexplored area of research. Continual decline of rab11 activation in trappc9 null mice would inevitably cause improper function of these cargo proteins in the brain.

How rab11 dysfunction relates to the disproportion of D1R and D2R containing neurons in trappc9 KO mice remains speculative. D2R but not D1R undergoes rab11-dependent recycling (*40*, *41*). Consistently, we found that levels of D2R on neuronal surfaces in brain sections of trappc9 KO mice were reduced relative to those in WT mice. Our finding supports the notion that endocytosed D2R was unable to efficiently return to cell surfaces, in other words, entrapped in recycling endosomes or delivered to lysosomes. Endocytosis of D2R can occur constitutively (no ligand binding) or be driven upon ligand engagement; only those D2R molecules endocytosed with ligands rely on rab11 for recycling back to cell surfaces, as recycling of constitutively endocytosed D2R molecules is regulated by rab4 (*40*). In this regard, dysfunction of D2R neurons would occur when prolonged stimulation of D2R is needed. This hypothesis is supported by our observation that the decrease of D2R neuronal density in trappc9 KO mice commenced after age p15, when motor activities of mice vastly increase and D2R activation/resensitization is in great need. Future studies are necessary to unveil signaling pathway(s) linking impaired recycling of D2R to cell death.

We noticed that female trappc9 KO mice displayed a broader range of behavioral deficits and appeared overweight earlier than male mice. Sexual differences are actually seen in many diseases including neuropsychiatric disorders. While sexual dimorphism involves complex interactions among sex hormones, genetic, and epigenetic factors, estrogens have been shown to influence a wide array of dopamine-dependent cognitive processes including object recognition and space/response memories (*43*), which are impaired in trappc9-deficient mice. Estrogens can increase the density of D2R on striatal neurons without changing levels of D2R mRNA (*43*), suggesting that estrogens speed up D2R recycling. As levels of estrogens differ greatly between female and male mice, neurons in female trappc9 KO mice require D2R recycling to cell surfaces more than neurons in male mice. In this regard, high levels of estrogens in female trappc9 KO mice could magnify the existing impairment of D2R recycling, thereby aggravating dysfunction of D2R neurons in female trappc9 KO mice.

Trappc9 null mice developed a broad range of behavioral defects and presented malformations of various brain structures. Our data suggest that the behavioral deficits resulted from an imbalance between D1R and D2R neurons in the striatum of trappc9 KO mice. However, we did not attempt to exclude the likelihood of the involvement of other populations of cells in the development of the functional defects. In the case of dopamine receptive neurons, we observed that levels of both D1R and D2R were significantly decreased in the hippocampus of trappc9 KO mice. Contrary to an increase in the striatum, the ratio of D1R to D2R neurons was decreased in the hippocampus of trappc9 KO mice. Rab11-independent recycling of D1R does not mean that rab11 is dispensable for D1R neurons. A significant decline in cross-sectional areas of D1R neurons in brain sections of trappc9 null mice supports the idea that rab11 dysfunction also impedes endocytic recycling in D1R neurons. Therefore, functional impairments of hippocampal D1R and D2R neurons may also contribute to poor performances of trappc9 null mice on cognitive tasks.

Glial cells may also be involved in the development of behavioral deficits seen in trappc9 KO mice. Astrogliosis is a defensive reaction of astrocytes in response to harmful stimuli and facilitates to restore homeostasis of the central nervous system, yet persistent astrogliosis can be detrimental and frequently occurs in neuropsychiatric disorders (*36*). Astrocytes not only regulate the formation, remodeling, and elimination of neuronal synapses but also communicate with oligodendrocytes to support myelination (*36*). We observed that astrogliosis in trappc9 KO mice appeared in the corpus callosum and the dentate gyrus, where neurogenesis takes place throughout life. It is necessary for future studies to clarify whether astrogliosis in trappc9 KO mice occurs as a normal response to slowed myelination and/or synaptogenesis or acts as a trigger of pathological changes. White matter hypoplasia and corpus callosum thinning are prominent pathological hallmarks in the brain of patients with ID with mutations in trappc9 as well as in other TRAPP subunits or rab11. We observed corpus callosum hypoplasia and decreased levels of oligo-2 in trappc9-deficient mice. It will be interesting to know whether and how trappc9 loss affects the proliferation and or maturation of oligodendrocytes. Further studies are also needed to evaluate

long-term effects of drugs acting on dopamine receptors on the improvement of brain functions in trappc9 KO mice. Nevertheless, the line of trappc9 null mice we report here provides a useful tool for addressing the above important issues, although this model may be limited in elucidating the specific role of trappc9 in the brain.

In summary, we describe a new mouse model that recapitulates features of human ID resulting from the deficiency of trappc9 and suggest a pathogenic mechanism and a potential therapy for improving brain function in individuals suffering from this disorder. Moreover, our study indicates that mTRAPP-II is a specific GEF for rab11 in mammals.

MATERIALS AND METHODS

Animals

All experimental procedures regarding the use of animals were conducted in accordance with National Institutes of Health (NIH) *Guide for the Care and Use of Laboratory Animals* and approved by the Institutional Animal Care and Use Committee of the Shanghai Jiao Tong University. Mice were housed in male and female groups under a normal 12-hour light/dark cycle (lights on at 7:00 a.m.) and a constant temperature with food and water ad libitum.

Generation of trappc9-deficient mice

We designed a pair of guide RNAs (gRNAs) (5′ gaacgccggagtgattgagc and 5′ atgctgtgtacatcaatctc) to generate trappc9-deficient mice, which had 109 nucleotides deleted from mouse trappc9 gene. The gRNAs targeted exon 7 of mouse trappc9 gene; this exon in human contains a disease-causative mutation present in multiple families. The production of cas9 mRNA and gRNAs by in vitro transcription and subsequent pronuclear injection and zygote transfer were carried out at Bioray Laboratories Inc., Shanghai. Primers designed for detecting the deletion mutation in trappc9 null mice were C9f, 5′ cccaaacccaaactcctctaa and C9r, 5′ actgctcgtccgaaagtcctg. Amplification with genotype primers was conducted with Taq polymerase (Thermo Fisher Scientific) for 30 cycles of 20 s at 95°C, 15 s at 55°C, and 40 s at 72°C with an initial denaturation at 95°C for 3 min and a final elongation at 72°C for 5 min. The length of polymerase chain reaction (PCR) products amplified from WT and mutant alleles was 667 and 558 base pairs, respectively. To minimize off-target effects, trappc9 mutant mice were backcrossed onto WT background for six generations. Genomic DNAs were prepared from toe tissues of a trappc9 mutant mouse of the sixth generation and used for verification of off-target mutations at or near the predicted sites. No off-target mutation was detected.

Protein purification

Glutathione *S*-transferase (GST), GST-dArab11, GST-dNrab11, GST-rab1-His, GST-rab5-His, or GST-rab11-His proteins were affinity-purified from bacteria with appropriate resins according to the manufacturer's instructions. Proteins tagged with both GST and 6×His were sequentially purified first with Ni–nitrilotriacetic acid (NTA) resins (Qiagen) and then with glutathione resins. All purified proteins were dialyzed and frozen in aliquots at −80°C until use.

Preparation of cellular membranes from mouse brains

Fresh brain tissues of WT and trappc9 KO mice aged at 10 to 12 weeks were harvested, minced into pieces, and homogenized on ice in lysis buffer containing 25 mM Hepes-Na (pH 7.4), 1 mM EDTA (pH 8.0), and 0.25 M sucrose with protease inhibitors (Roche) by passing through a dounce homogenizer. Homogenates were briefly centrifuged to remove debris and nuclei. The resulting supernatants were placed on a gradient prepared in an SW41 tube with 0.5 M sucrose and 80% glycerol and centrifuged at 4°C, 41,000 rpm for 1 hour in an SW41 rotor (Beckman-Coulter). Membranes at interfaces between 0.5 M sucrose and 80% glycerol were collected, extracted with Triton X-100, and used for pull-down or nucleotide exchange assay after determining protein concentrations.

Pull-down assays

To look for proteins potentially interacting with rab11, GST-dNrab11, GST-dArab11, or GST was immobilized on glutathione resins and incubated with Triton X-100 solubilized mouse brain membranes. After washes, proteins on glutathione resins were eluted into SDS–polyacrylamide gel electrophoresis (SDS-PAGE) sample buffers and analyzed by SDS-PAGE followed by silver staining or Western blot with indicated antibodies. Gel slices containing silver-stained protein bands were cut out, treated with trypsin, and analyzed by mass spectrometry at the Harvard Mass Spectrometry Core Facility.

To enrich mTRAPP-II, total cellular membranes were prepared from human embryonic kidney–293T cells infected with lentivirus *bi*-cistronically expressing GFP and S-tagged trappc9 (Open Biosystems) or empty lentivirus (Mock). Triton X-100 solubilized cellular membranes were incubated with S-protein resins (Novagen). After washes, mTRAPP-II on S-protein resins were either eluted for SDS-PAGE analysis or resuspended in exchange buffers for use in nucleotide exchange assays.

Guanine nucleotide exchange assays

[^{3}H]GDP (11.9 Ci/mmol, GE Life Sciences) and 2′-(3′)-bis-*O*-(*N*-methylanthraniloyl)-GDP (mant-GDP, Molecular Probes) were used as tracers of nucleotide exchange. Rab proteins (rab1, rab5, and rab11) tagged with both GST and 6×His were separately loaded with [^{3}H]GDP or mant-GDP in buffers containing 20 mM Hepes (pH 7.2), 20 mM potassium acetate, 1 mM dithiothreitol (DTT), 5 mM EDTA, and 0.05% Triton X-100 at 30°C for 30 min and then incubated with Ni-NTA beads after adding $MgCl_2$ to a final concentration of 10 mM. After a brief centrifugation, supernatants containing unbound [^{3}H]GDP or mant-GDP were discarded. Loaded rabs on Ni-NTA beads were washed and resuspended in assay buffers containing 20 mM Hepes (pH 7.4), 150 mM NaCl, 5 mM $MgCl_2$, 1 mM DTT, and 0.5 mM GTP/GDP. After GEF samples in assay buffers were mixed with [^{3}H]GDP or mant-GDP loaded rabs, nucleotide exchange reactions were conducted at 30°C for indicated times ([^{3}H]GDP release) or at room temperature in a multimode microplate spectrophotometer. After reactions were terminated, [^{3}H]GDP-rab proteins on Ni-NTA beads were collected by a brief centrifugation, washed, and subjected for scintillation counting. Data were represented as means ± SD percentage of [^{3}H]GDP release (total [^{3}H]GDP bound on rabs minus [^{3}H]GDP remained on rabs after reactions).

For mant-GDP release, 25, 50, and 100 μg of brain membranes (WT versus KO) were mixed with rab proteins loaded with mant-GDP to initiate GEF reactions. In each set of GEF reactions, controls included reactions containing only equal amounts of brain membranes (WT versus KO), mant-GDP loaded rab proteins alone, and 5 mM EDTA with mant-GDP loaded rab proteins. Fluorescence signals in all reactions were measured over 30 min on a Tecan Infinite M200 PRO multimode microplate spectrophotometer with excitation

at 360 nm and emission at 440 nm. Average intensities of fluorescent signals measured over 20 min in reactions containing WT or trappc9 KO mouse brain membranes only were calculated and used as the background signals. After removing the corresponding background signals, values of fluorescence intensities measured at each time point in GEF reactions containing loaded rab proteins and brain membranes as well as values of fluorescence signals obtained from reactions with loaded rab proteins alone were used for determining the observed pseudo–first-order rate constants (k_{obs}) by nonlinear regression fit to the one-phase exponential decay with the aid of the Prism 8.0 (GraphPad Software Inc.). A set of GEF reactions was carried out using brain membranes prepared from one WT and one age-matched trappc9 KO mouse.

Mouse primary neuronal and embryonic fibroblast cultures

Primary neurons were prepared from cortices including striata of E18 embryos of WT and trappc9 KO mice, whereas primary MEFs were prepared from E13 to E14 embryos of WT and trappc9 KO mice with standard procedures. The genotype of each embryo was determined by PCR with C9f and C9r primers as above. Primary neurons were cultured at 37°C in a cell culture incubator in Dulbecco's modified Eagle's medium (DMEM)/F12 supplemented with 10% fetal bovine serum (FBS), 1× Glutamax, 1× penicillin/streptomycin, and 1× NEAA for 24 hours and then changed into Neurobasal DMEM media containing B27 supplement, Glutamax, and penicillin/streptomycin. Thenceforth, one-half of fresh media was changed every 3 days. MEFs used for fluorescence microscopy were seeded on glass coverslips the day before being processed for immunolabeling with antibodies against rab1 (rabbit polyclonal, 1:250; Cell Signaling, D5F8M), rab11 (mouse monoclonal, 1:250; BD Transduction Laboratories, 610657), or GM130 (mouse monoclonal, 1:250; BD Transduction Laboratories, 610823). Rhodamine Red–conjugated secondary antibodies (the Jackson Laboratory) were used for detection. Before mounting onto glass slides for fluorescence microscopy, MEFs on coverslips were stained with Hoechst 34580.

Transferrin uptake and recycling assay

Primary neurons at 7 to 9 days in vitro were completely cooled down on ice by washes in cold phosphate-buffered saline, changed into fresh cold serum-free DMEM containing Alexa 568–transferrin (10 μg ml^{-1}; Invitrogen), and incubated on ice for 30 min to allow Alexa 568–transferrin to bind to its receptors on cell surfaces. Neurons labeled with Alexa 568–transferrin were either directly fixed (total binding) or incubated at 37°C for 5, 15, or 30 min and then fixed for fluorescence microscopy. Digital images were captured using the Olympus BX51 microscopy imaging system with the same settings for all conditions. Intensities of Alexa 568–transferrin signals in somata of neurons and the corresponding background signals were measured using NIH ImageJ. Data were represented as means ± SD intensities of Alexa 568–transferrin signals.

Western blot analysis

Samples used for Western blot analysis in this study were precipitated proteins or protein lysates prepared from brain tissues of WT and trappc9 KO mice in buffers containing protease and phosphatase inhibitors (B14011 and B15001, Bimake). Equal amounts of proteins were analyzed by SDS-PAGE and Western blot. Primary antibodies used for Western blot analysis included rabbit anti-trappc9 (1:500; Abcam, ab104041), rabbit anti-trappc2 (1:1000; Abcam, ab111848), mouse anti-trappc4 (1:500; Santa Cruz, sc-390551), mouse anti-trappc10 (1:500; Santa Cruz, sc-101259), rabbit anti-trappc11 (1:500; Biorbyt, orb186301), rabbit anti-rab1a (1:1000; Cell Signaling, D5F8M), mouse anti-rab4 (1:1000; BD Transduction Laboratories, 610889), rabbit anti-rab5 (1:500; Invitrogen, PA5-29022), rabbit anti-rab7 (1:500; Invitrogen, PA5-23138), mouse anti-rab11 (1:1000; BD Transduction Laboratories, 610657), mouse anti-rab18 (1:500; Santa Cruz, sc-393168), rabbit anti-NIK (1:1000; Abcam, ab216409), NF-κB Pathway Sampler Kit [1:1000, Cell Signaling, 9936, including IκB kinase α (IKKα), IKKβ, phospho-IKKα/β on Ser^{176}/180, phospho-p65 on Ser^{536}, IκBα, phospho-IκBα on Ser^{32}, and p65], mouse anti-NeuN (1:1000; Millipore, MAB377), mouse anti-GFAP (1:1000; Millipore, MAB3402), goat anti-Iba1 (1:1000; Abcam, ab5076), mouse anti-Olig2 (1:500; Millipore, MABN50), rabbit anti-D1 receptor (1:1000; Abcam, ab20066), rabbit anti-D2 receptor (1:1000; Millipore, AB5084P), rabbit anti-DARPP32 (1:5000; Abcam, ab40801), and mouse anti–glyceraldehyde-3-phosphate dehydrogenase (GAPDH) (1:5000; Millipore, MAB374). Alexa Fluor 790– or 680–conjugated secondary antibodies were from Jackson ImmunoResearch Laboratories (1:50,000; 111-655-144, 705-625-147, and 115-625-146). Blots were imaged with the Odyssey P140-CLx Infrared Imaging system (LI-COR Biosciences). Digital images with signals of protein bands in linear ranges were used for densitometry quantification with the aid of NIH ImageJ.

Immunohistochemistry

Mice at the age of 10 to 12 weeks were deeply anesthetized and transcardially perfused with 50 ml of phosphate saline followed by 50 ml of 4% (w/v) paraformaldehyde (Sigma-Aldrich) in 0.1 M in phosphate buffer (pH 7.4). Fixed brains of WT and trappc9 KO mice were cut into 30- or 50-μm-thick coronal or sagittal sections on a cryostat (Leica CM1950) or a vibratome (Leica VT1000S). We used 30-μm-thick coronal sections cut from bregma 3.56 mm for examining D1R (83rd to 85th), D2R (98th to 100th), and DARPP32 (95th to 97th) to compare cell densities and or expression levels, and 50-μm-thick coronal sections cut from bregma 3.56 mm and through the hippocampus for detecting trappc9 in astrocytes (107th to 109th) or neurons (114th to 116th). Immunolabeling was performed with free-floating brain sections. For labeling D1R and D2R, Triton X-100 was omitted in all buffers. After labeling with antibodies, brain sections were processed for detection with the avidin-biotin peroxidase method (Vectastain Elite ABC kit, Vector Laboratories) and subsequently mounted onto glass slides with Cytoseal (Thermo Fisher Scientific). Digital images were acquired with a DP-72 CCD camera on an Olympus BX51 microscope using the Olympus imaging software. For detecting trappc9 in neurons (NeuN) or astrocytes (GFAP), secondary antibodies conjugated with different fluorescent dyes were used. Cells in brain sections were identified by Hoechst 34580 staining of nuclei. Brain sections were mounted onto glass slides with ProLong Gold (Invitrogen) for fluorescence microscopy. Digital images were acquired through a DP-72 CCD camera on an Olympus BX51 microscope or with the Leica TCS SP5 confocal imaging system with the same settings for all conditions. Primary antibodies for immunohistochemistry were rabbit anti-D1R [1:1000, customer made in the DiFiglia Laboratory (*44*)], rabbit anti-D2R (1:500; Millipore, AB5084P), rabbit anti-DARPP32 (1:1000; Chemicon, AB1656), rabbit anti-trappc9 (1:250; Abcam, ab104041), mouse anti-GFAP (1:400; Millipore, MAB3402), and mouse anti-NeuN (1:100; Millipore, MAB377). Secondary antibodies were as follows: biotinylated

goat anti-rabbit (1:500; Vector Laboratories, BA-1000), goat anti-mouse immunoglobulin G (IgG)(H + L), BODIPY FL (1:500; Invitrogen, B-2752), and donkey anti-rabbit IgG(H + L). Rhodamine Red (1:200; the Jackson Laboratory, 711-295-152) was used for detection.

Luxol fast blue staining

A series of consecutive 30-μm-thick sagittal sections cut from lateral 0.12 mm (31st to 33rd) were mounted on polylysine-coated slides, dried in air, and processed for luxol fast blue (LFB) staining. Brain sections on slides were dehydrated by being soaked sequentially in 50, 70, 80, 95, and 100% ethanol and then incubated with 0.1% LFB in 95% ethanol at 60°C for 30 min. After being cooled down at room temperature, the slices were rehydrated and then soaked in 0.05% lithium carbonate if sections were overstained. Slices were dehydrated as above and cleared twice in xylene each for 5 min before being covered with Dibutylphthalate Polystyrene Xylene (DPX) and glass coverslips. Stained brain sections were examined under an Olympus BX51 microscope and images were collected with a DP-72 CCD camera mounted on the microscope using the OLYMUPUS cellSens Entry software.

Image analysis and stereology quantification

For measuring the volume of specific brain structures in LFB-stained brain sections, images were collected from three consecutive sagittal sections of each brain through an Olympus LMPLFLN 4× objective. Images were captured from three consecutive coronal sections of each animal through an LMPLFLN 10× objective and used for determining the density of DARPP32-, D1R-, or D2R-positive cells. For measuring fluorescence intensities of GFAP signals and contents of NeuN-positive cells in brain sections, images were captured through a Leica 10× objective. Images used for determining levels of D1R and D2R on cell surfaces were captured through a 20× objective with the Olympus BX51 microscopy imaging system. Images used for analysis using NIH ImageJ were converted to 8-bit black-and-white images, with background signals removed from the corresponding images. All quantitative analyses were conducted by two investigators blinded to experimental conditions.

We used images captured from LFB-stained sagittal brain sections for measuring the volume of brain structures. A given brain structure was circumscribed using the "freehand selection" tool and measured using the "measure" function to obtain the cross-sectional area and to estimate the volume based on the section thickness and number of sections analyzed. To quantify intensities of GFAP immunoreactive signals in specific brain regions, each of the specific brain structures in a brain section was circumscribed using freehand selection. The cross-sectional area of each brain structure and the signal intensities within the corresponding brain structure were obtained using the measure function. Data were expressed as means ± SD of signal intensities per area.

To quantify the number of DARPP32-, D1R-, D2R-, and NeuN-positive cells, the striatum or nucleus accumbens or other brain structures were demarcated using the freehand selection tool. The cross-sectional area of the chosen area in each brain section of each animal was measured with the measure function and converted into square millimeters based on the resolution of the images used for the analysis. We calculated the volume of a brain structure in a brain section simply by multiplying the measured cross-sectional area by the thickness of the brain section (30 μm). Labeled cells in a given brain structure from each section of each animal were manually counted using the "multipoint" tool. Data were represented as means ± SD of cell number per cubic millimeter. To determine whether neuronal loss occurs in the hippocampus, we measured the thickness of the pyramidal cell layer of CA1 to CA3 and the granular cell layer of the dentate gyrus.

To determine levels of D1R and D2R on neuronal surfaces, we chose those neurons with a clear edge for analysis in consideration that not all neurons were in focus. The outer and inner edges of the soma of a neuron were tracked using the freehand selection tool to generate two contours. Signal intensities within the outer and inner contours for each neuron were measured separately. The difference of signals within the two contours were determined and used for calculating the ratio to intensities of signals within the outer contour. This ratio from each neuron was designated as levels of D1R or D2R on the surface of that neuron. Cross-sectional areas of the outer contour of each chosen neuron were also measured and converted to square micrometers based on the actual resolution of the image. This value in square micrometers was used for representing the size of that neuron.

Mouse behavior tests

The mice were housed in gender groups. All behavioral tests starting from 8 weeks of age were performed between 8 p.m. and 4 a.m. under standard laboratory conditions (at 23° ± 2°C and relative humidity of 45 to 50%). All mice were transferred to the testing room to acclimate at least 1 hour before each behavioral test. Two different tests for each animal were separated by 48 hours to prevent one test from interfering with the other. All testing apparatuses were cleaned with 70% alcohol and distilled water to eliminate residual odors before each animal was assessed. In all behavioral tests, animals were randomly chosen. Experimenters who conducted behavioral tests and data analyses were blinded to the genotype of animals. Behavioral tests were conducted in the following order: grip strength, rotarod, open field, novel object recognition, elevated plus maze, three-chamber social interaction, Morris water maze, and tail suspension. After all behavioral tests were completed, and a subgroup of WT and trappc9 KO mice were euthanized for biochemical and histochemical studies.

Grip strength test

The grip strength of mice was measured using a mouse grip strength meter according to the manufacturer's instructions (YLS-13A, Jinan Yiyan Scientific Research Company, Shandong, China). In brief, one of the two experimenters held the middle part of the mouse tail and horizontally pulled the animal back with even force until the mouse withdrew its paws from the dynamometer. The dynamometer automatically recorded the maximal grip strength. The grip strength of six attempts was averaged.

Accelerated rotarod test

The rotarod apparatus was a five-station rotarod treadmill (YLS-4C, Jinan Yiyan Scientific Research Company, Shandong, China) and was set to accelerate from 4 to 40 rpm over 5 min. Each test consisted of three trials with an interval of 30 min for each animal. Each mouse was evaluated over the course of 8 days (24 total trials). Before the first trial, all animals were left on the rod for 60 s. During any trial, mice that turned 180° to face backward (the same direction as rotation) were gently guided to turn around to face forward (opposite direction of rotation). The trial was terminated when a mouse fell off. Time and speed to fall off were recorded for each mouse.

Open field test

The open field is a white wooden box [80 cm (length) by 80 cm (width) by 30 cm (depth)] divided into 16 identical squares on the

floor and surmounted with a video camera, which was connected to a computer located in a nearby room. Each mouse was placed individually in the same arena and allowed to freely explore for 5 min. The performance of each mouse was automatically monitored with the video camera. The total distance traversed and the time spent in central areas (20 cm by 20 cm) of the arena were automatically scored using the installed Smart video tracking system (MobileDatum, China).

Novel object recognition test

The novel object recognition test is composed of three test sessions spread in 3 days. In each testing session, the mouse was allowed to explore in the box for 5 min. On the first day, no object was placed in the box. On the second day, two identical objects were placed at different loci of the box. On the third day, a novel object of different shape and color was introduced to replace one of the two identical objects. To exclude effects of olfactory cues, the box and the objects were thoroughly cleaned with 70% ethanol and distilled water after each trial. Object exploration time was defined as the length of time spent in sniffing or touching the object with the nose and/or forepaws within 2 cm from the object. Sitting or standing on the object was not considered as exploration. Exploratory activities of each mouse in each test session were recorded with an overhead video camera and scored by two experienced observers blinded to the genotype of mice.

Elevated plus maze test

The elevated plus maze apparatus consisted of two open arms [30 cm (length) by 5 cm (width) by 0.3 cm (height)] and two closed arms [30 cm (length) by 5 cm (width) by 15 cm (height)], which extended from the central platform [5 cm (length) by 5 cm (height)]. The maze was elevated 50 cm above the floor with a video camera placed on top of it. Each mouse was gently placed in the center of the platform with the head facing one of the open arms and allowed to explore for 5 min. Mouse behaviors were recorded with the overhead video camera. The time spent in each arm and the number of entries into each arm was automatically scored with the video tracking system (Smart video tracking system, MobileDatum, China). The percentage of time spent in the open arms and the percentage of frequencies of entry into the open arms were calculated based on the total time and total number of entries.

Three-chamber social interaction test

The three-chamber social interaction test was conducted in a clear rectangular plastic box [60 cm (length) by 40 cm (width) by 22 cm (height)], which was divided into three equal-sized chambers [20 cm (length) by 40 cm (width) each] with a door open to the chamber on either side. Both familiar and stranger animals were WT mice with the same age and gender as the test mouse and habituated to the inverted wire cups for 1 hour before experiments. The inverted wire cups were cylindrical, 10 cm in height, with a bottom diameter of 10 cm. A weighted bottle was placed on top of the inverted cups to prevent mice from climbing onto the cup. The chambers and wire cups were cleaned with 70% ethanol and water before and after each test. Test mice were habituated to the facility for 1 hour before the start of the test. During the habituation phase, the test mouse was placed into the middle chamber and allowed to explore all three empty chambers for 5 min. During the sociability test phase, the test mouse was first placed in the middle chamber with the doors to both side chambers closed, and a familiar mouse was placed under the inverted wire cup in one of the side chambers and an object under the inverted wire cup in the opposite side chamber. The location of the familiar mouse and the object was counterbalanced between test trials to exclude side preference. The observer then lifted the doorways to both side chambers simultaneously, and the test mouse was allowed to explore all three chambers for 5 min. During the social novelty test phase, the test mouse was again gently placed into the middle chamber with the doors closed. Then, a stranger mouse was placed under the wire cup in the other side chamber opposite to the familiar mouse. After the doorways to both side chambers were lifted simultaneously, the test mouse was allowed to explore all three chambers for 5 min. Activities of test mice were recorded with a video camera above. The time spent in interacting with each inverted wire cup was automatically scored with the video tracking system (Smart video tracking system, MobileDatum, China). Two investigators blinded to the genotype of the tested mice evaluated manually to ensure the accuracy of automatic scorings.

Morris water maze test

The Morris water maze test was carried out in a white circular pool with a diameter of 120 cm and a height of 40 cm, filled with 23° ± 2°C opaque water. The test consisted of a 2-trial visible platform phase (1 day) and a 20-trial hidden platform phase (5 days) followed by a 1-trial probe phase (1 day). During the visible platform phase, a visible platform (9 cm in diameter) was placed 1 cm above the water surface and a red flag on a plastic cap was placed on the platform to increase the visibility. During the hidden platform phase, the platform was submerged 1 cm below the water surface and placed in the middle of the southwest quadrant. The pool was in a dimly lit room with various external cues and topped with a video camera that was connected to a computer in a nearby room. The visible platform test phase was composed of two trials, each for 60 s, with an interval of 30 min between trials. The hidden platform test phase in each day for each animal was composed of four trials, each for 60 s, with an intertrial interval of 30 min. Each mouse was tested for five consecutive days. During the interval of trials, the test mouse was placed back in the home cage. In each of the four trials, the test mouse was placed into a different quadrant of the pool to exclude spatial preference. If it failed to find the submerged platform within 60 s, the mouse was placed on the platform to have a rest for 15 s. If it found the platform, the mouse was allowed to stay on the platform for 15 s. The probe trial was performed the day after the last trial session of the hidden platform test phase. During the probe test phase, the platform was removed, and the mouse was placed in the quadrant diagonal to the platform quadrant and allowed to search for the platform for 60 s. Behaviors of each mouse in each trial were recorded using the automated tracking system (Smart video tracking system, MoblieDatum, China). The latency to reach the platform, the speed of swim (cm/s), and the frequency of crossing the original locus of the hidden platform, as well as the duration of swimming in the platform quadrant (probe trial), were measured.

Tail suspension test

The tail suspension test apparatus consisted of a metal frame [60 cm (height) by 72 cm (width) by 15 cm (depth)] with a metal rod above (1.5 cm in width) and was separated into four acoustically and visually isolated compartments in equal width so that four animals could be assessed simultaneously. To prevent tail climbing, mice were suspended with their tails immobilized on the above metal rod with adhesive tapes. Immobility was considered as a state of the animal with no visible voluntary movement (less than 1 cm) of its head, body, or limbs within 5 s or more. Involuntary swinging was considered as immobility. Each test for each animal lasted for 6 min. Behaviors of each mouse were recorded with a video camera, and

the immobility time within the past 4 min of the test was analyzed and scored by two experienced researchers blinded to the genotype of the tested animals.

Pharmacological treatment studies

We first determined an optimal time for detecting drug effects by evaluating exploratory activities of trappc9 KO mice in an open field at 0.5, 3, 6, 12, 24, and 48 hours after intraperitoneal injection of SCH23390 (0.1 mg/kg; Tocris, 0925), quinpirole (1 mg/kg; Tocris, 1061), or in combination. As exploratory activities of trappc9 KO mice were raised to levels of WT mice upon treatment with both chemicals for 24 hours, we conducted novel object recognition, three-chamber social interaction, and Morris water maze tests to evaluate drug effects in trappc9 KO mice on these tasks 24 hours after a dose of each of SCH23390 and quinpirole was given. For Morris water maze test, each mouse was evaluated for six consecutive days and thus given six doses of each of SCH23390 and quinpirole in total. Behavioral tests were conducted with an interval of 72 hours between different tests to prevent one test from interfering with the other. Procedures of behavioral tests were the same as above.

Statistical analysis

All statistical analyses were executed using the Prism v.8.0 (GraphPad Software Inc.). Two-tailed unpaired Student's *t* test was conducted to compare two groups, whereas one-way analysis of variance (ANOVA) and/or repeated-measures ANOVA followed by Tukey's test was used for comparison among multiple groups. All data were expressed as means ± SD unless otherwise noted. $P < 0.05$ was statistically significant.

SUPPLEMENTARY MATERIALS

Supplementary material for this article is available at http://advances.sciencemag.org/cgi/content/full/6/47/eabb7781/DC1

View/request a protocol for this paper from *Bio-protocol*.

REFERENCES AND NOTES

1. A. K. Srivastava, C. E. Schwartz, Intellectual disability and autism spectrum disorders: Causal genes and molecular mechanisms. *Neurosci. Biobehav. Rev.* **46** (Pt 2), 161–174 (2014).
2. A. A. Abbasi, K. Blaesius, H. Hu, Z. Latif, S. Picker-Minh, M. N. Khan, S. Farooq, M. A. Khan, A. M. Kaindl, Identification of a novel homozygous *TRAPPC9* gene mutation causing non-syndromic intellectual disability, speech disorder, and secondary microcephaly. *Am. J. Med. Genet. B Neuropsychiatr. Genet.* **174**, 839–845 (2017).
3. A. Hnoonual, P. Graidist, S. Kritsaneepaiboon, P. Limprasert, Novel compound heterozygous mutations in the *TRAPPC9* gene in two siblings with autism and intellectual disability. *Front. Genet.* **10**, 61 (2019).
4. G. Marangi, V. Leuzzi, F. Manti, S. Lattante, D. Orteschi, V. Pecile, G. Neri, M. Zollino, *TRAPPC9*-related autosomal recessive intellectual disability: Report of a new mutation and clinical phenotype. *Eur. J. Hum. Genet.* **21**, 229–232 (2013).
5. A. Mir, L. Kaufman, A. Noor, M. M. Motazacker, T. Jamil, M. Azam, K. Kahrizi, M. A. Rafiq, R. Weksberg, T. Nasr, F. Naeem, A. Tzschach, A. W. Kuss, G. E. Ishak, D. Doherty, H. H. Ropers, A. J. Barkovich, H. Najmabadi, M. Ayub, J. B. Vincent, Identification of mutations in *TRAPPC9*, which encodes the NIK- and IKK-β-binding protein, in nonsyndromic autosomal-recessive mental retardation. *Am. J. Hum. Genet.* **85**, 909–915 (2009).
6. G. H. Mochida, M. Mahajnah, A. D. Hill, L. Basel-Vanagaite, D. Gleason, R. S. Hill, A. Bodell, M. Crosier, R. Straussberg, C. A. Walsh, A truncating mutation of *TRAPPC9* is associated with autosomal-recessive intellectual disability and postnatal microcephaly. *Am. J. Hum. Genet.* **85**, 897–902 (2009).
7. O. Philippe, M. Rio, A. Carioux, J.-M. Plaza, P. Guigue, F. Molinari, N. Boddaert, C. Bole-Feysot, P. Nitschke, A. Smahi, A. Munnich, L. Colleaux, Combination of linkage mapping and microarray-expression analysis identifies NF-κB signaling defect as a cause of autosomal-recessive mental retardation. *Am. J. Hum. Genet.* **85**, 903–908 (2009).
8. Z. Bai, X. Kong, Diagnosis of a case with mental retardation due to novel compound heterozygous variants of *TRAPPC9* gene. *Zhonghua Yi Xue Yi Chuan Xue Za Zhi* **36**, 1115–1119 (2019).
9. K. M. Wilton, L. B. Gunderson, L. Hasadsri, C. P. Wood, L. A. Schimmenti, Profound intellectual disability caused by homozygous *TRAPPC9* pathogenic variant in a man from Malta. *Mol. Genet. Genomic Med.* , e1211 (2020).
10. N. Krumm, T. N. Turner, C. Baker, L. Vives, K. Mohajeri, K. Witherspoon, A. Raja, B. P. Coe, H. A. Stessman, Z.-X. He, S. M. Leal, R. Bernier, E. E. Eichler, Excess of rare, inherited truncating mutations in autism. *Nat. Genet.* **47**, 582–588 (2015).
11. J. Li, L. Wang, H. Guo, L. Shi, K. Zhang, M. Tang, S. Hu, S. Dong, Y. Liu, T. Wang, P. Yu, X. He, Z. M. Hu, J. Zhao, C. Liu, Z. S. Sun, K. Xia, Targeted sequencing and functional analysis reveal brain-size-related genes and their networks in autism spectrum disorders. *Mol. Psychiatr.* **22**, 1282–1290 (2017).
12. M. Klein, E. L. Singgih, A. van Rens, D. Demontis, A. D. Børglum, N. R. Mota, A. Castells-Nobau, L. A. Kiemeney, H. G. Brunner, A. Arias-Vasquez, A. Schenck, M. van der Voet, B. Franke, Contribution of intellectual disability–related genes to ADHD risk and to locomotor activity in *Drosophila*. *Am. J. Psychiatry* **177**, 526–536 (2020).
13. S. E. McCarthy, J. Gillis, M. Kramer, J. Lihm, S. Yoon, Y. Berstein, M. Mistry, P. Pavlidis, R. Solomon, E. Ghiban, E. Antoniou, E. Kelleher, C. O'Brien, G. Donohoe, M. Gill, D. W. Morris, W. R. McCombie, A. Corvin, De novo mutations in schizophrenia implicate chromatin remodeling and support a genetic overlap with autism and intellectual disability. *Mol. Psychiatr.* **19**, 652–658 (2014).
14. Z. Lipatova, N. Segev, Ypt/Rab GTPases and their TRAPP GEFs at the Golgi. *FEBS Lett.* **593**, 2488–2500 (2019).
15. M. C. Bassik, M. Kampmann, R. J. Lebbink, S. Wang, M. Y. Hein, I. Poser, J. Weibezahn, M. A. Horlbeck, S. Chen, M. Mann, A. A. Hyman, E. M. Leproust, M. T. McManus, J. S. Weissman, A systematic mammalian genetic interaction map reveals pathways underlying ricin susceptibility. *Cell* **152**, 909–922 (2013).
16. C. Li, X. Luo, S. Zhao, G. K. Siu, Y. Liang, H. C. Chan, A. Satoh, S. S. Yu, COPI-TRAPPII activates Rab18 and regulates its lipid droplet association. *EMBO J.* **36**, 441–457 (2017).
17. F. Riedel, A. Galindo, N. Muschalik, S. Munro, The two TRAPP complexes of metazoans have distinct roles and act on different Rab GTPases. *J. Cell Biol.* **217**, 601–617 (2018).
18. A. Yamasaki, S. Menon, S. Yu, J. Barrowman, T. Meerloo, V. Oorschot, J. Klumperman, A. Satoh, S. Ferro-Novick, mTrs130 is a component of a mammalian TRAPPII complex, a Rab1 GEF that binds to COPI-coated vesicles. *Mol. Biol. Cell* **20**, 4205–4215 (2009).
19. L. L. Thomas, J. C. Fromme, GTPase cross talk regulates TRAPPII activation of Rab11 homologues during vesicle biogenesis. *J. Cell Biol.* **215**, 499–513 (2016).
20. N. Bögershausen, N. Shahrzad, J. X. Chong, J.-C. von Kleist-Retzow, D. Stanga, Y. Li, F. P. Bernier, C. M. Loucks, R. Wirth, E. G. Puffenberger, R. A. Hegele, J. Schreml, G. Lapointe, K. Keupp, C. L. Brett, R. Anderson, A. Hahn, A. M. Innes, O. Suchowersky, M. B. Mets, G. Nürnberg, D. R. M. Leod, H. Thiele, D. Waggoner, J. Altmüller, K. M. Boycott, B. Schoser, P. Nürnberg, C. Ober, R. Heller, J. S. Parboosingh, B. Wollnik, M. Sacher, R. E. Lamont, Recessive TRAPPC11 mutations cause a disease spectrum of limb girdle muscular dystrophy and myopathy with movement disorder and intellectual disability. *Am. J. Hum. Genet.* **93**, 181–190 (2013).
21. R. Harripaul, N. Vasli, A. Mikhailov, M. A. Rafiq, K. Mittal, C. Windpassinger, T. I. Sheikh, A. Noor, H. Mahmood, S. Downey, M. Johnson, K. Vleuten, L. Bell, M. Ilyas, F. S. Khan, V. Khan, M. Moradi, M. Ayaz, F. Naeem, A. Heidari, I. Ahmed, S. Ghadami, Z. Agha, S. Zeinali, R. Qamar, H. Mozhdehipanah, P. John, A. Mir, M. Ansar, L. French, M. Ayub, J. B. Vincent, Mapping autosomal recessive intellectual disability: Combined microarray and exome sequencing identifies 26 novel candidate genes in 192 consanguineous families. *Mol. Psychiatry* **23**, 973–984 (2017).
22. I. Marin-Valencia, G. Novarino, A. Johansen, B. Rosti, M. Y. Issa, D. Musaev, G. Bhat, E. Scott, J. L. Silhavy, V. Stanley, R. O. Rosti, J. W. Gleeson, F. B. Imam, M. S. Zaki, J. G. Gleeson, A homozygous founder mutation in *TRAPPC6B* associates with a neurodevelopmental disorder characterised by microcephaly, epilepsy and autistic features. *J. Med. Genet.* **55**, 48–54 (2017).
23. M. P. Milev, M. E. Grout, D. Saint-Dic, Y.-H. Cheng, I. A. Glass, C. J. Hale, D. S. Hanna, M. O. Dorschner, K. Prematilake, A. Shaag, O. Elpeleg, M. Sacher, D. Doherty, S. Edvardson, Mutations in *TRAPPC12* manifest in progressive childhood encephalopathy and Golgi dysfunction. *Am. J. Hum. Genet.* **101**, 291–299 (2017).
24. H. S. Mohamoud, S. Ahmed, M. Jelani, N. Alrayes, K. Childs, N. Vadgama, M. M. Almramhi, J. Y. Al-Aama, S. Goodbourn, J. Nasir, A missense mutation in *TRAPPC6A* leads to build-up of the protein, in patients with a neurodevelopmental syndrome and dysmorphic features. *Sci. Rep.* **8**, 2053 (2018).
25. N. J. Van Bergen, Y. Guo, N. Al-Deri, Z. Lipatova, D. Stanga, S. Zhao, R. Murtazina, V. Gyurkovska, D. Pehlivan, T. Mitani, A. Gezdirici, J. Antony, F. Collins, M. J. H. Willis, Z. H. Coban Akdemir, P. Liu, J. Punetha, J. V. Hunter, S. N. Jhangiani, J. M. Fatih, J. A. Rosenfeld, J. E. Posey, R. A. Gibbs, E. Karaca, S. Massey, T. G. Ranasinghe, P. Sleiman, C. Troedson, J. R. Lupski, M. Sacher, N. Segev, H. Hakonarson, J. Christodoulou, Deficiencies in vesicular transport mediated by *TRAPPC4* are associated with severe syndromic intellectual disability. *Brain* **143**, 112–130 (2020).

26. M. Langen, S. Durston, W. G. Staal, S. J. M. C. Palmen, H. van Engeland, Caudate nucleus is enlarged in high-functioning medication-naive subjects with autism. *Biol. Psychiatry* **62**, 262–266 (2007).
27. A. C. Kreitzer, R. C. Malenka, Striatal plasticity and basal ganglia circuit function. *Neuron* **60**, 543–554 (2008).
28. K. M. Money, G. D. Stanwood, Developmental origins of brain disorders: Roles for dopamine. *Front. Cell. Neurosci.* **7**, 260 (2013).
29. J. Cox, I. B. Witten, Striatal circuits for reward learning and decision-making. *Nat. Rev. Neurosci.* **20**, 482–494 (2019).
30. R. A. McCutcheon, A. Abi-Dargham, O. D. Howes, Schizophrenia, dopamine and the striatum: From biology to symptoms. *Trends Neurosci.* **42**, 205–220 (2019).
31. R. Emsley, L. Asmal, S. du Plessis, B. Chiliza, M. Kidd, J. Carr, M. Vink, Dorsal striatal volumes in never-treated patients with first-episode schizophrenia before and during acute treatment. *Schizophr. Res.* **169**, 89–94 (2015).
32. C. C. Robinett, M. G. Giansanti, M. Gatti, M. T. Fuller, TRAPPII is required for cleavage furrow ingression and localization of Rab11 in dividing male meiotic cells of *Drosophila*. *J. Cell Sci.* **122**, 4526–4534 (2009).
33. S. Scheggi, M. G. De Montis, C. Gambarana, DARPP-32 in the orchestration of responses to positive natural stimuli. *J. Neurochem.* **147**, 439–453 (2018).
34. A. J. Duszkiewicz, C. G. McNamara, T. Takeuchi, L. Genzel, Novelty and dopaminergic modulation of memory persistence: A tale of two systems. *Trends Neurosci.* **42**, 102–114 (2019).
35. T. Ott, A. Nieder, Dopamine and cognitive control in prefrontal cortex. *Trends Cogn. Sci.* **23**, 213–234 (2019).
36. M. Pekny, M. Pekna, Astrocyte reactivity and reactive astrogliosis: Costs and benefits. *Physiol. Rev.* **94**, 1077–1098 (2014).
37. K. Sato, A. Sakaguchi, M. Sato, REI/SH3BP5 protein family: New GEFs for Rab11. *Cell Cycle* **15**, 767–769 (2016).
38. I. J. C. Lamers, M. R. F. Reijnders, H. Venselaar, A. Kraus, D. D. D. Study, S. Jansen, B. B. A. de Vries, G. Houge, G. A. Gradek, J. Seo, M. Choi, J. H. Chae, I. van der Burgt, R. Pfundt, S. J. F. Letteboer, S. E. C. van Beersum, S. Dusseljee, H. G. Brunner, D. Doherty, T. Kleefstra, R. Roepman, Recurrent de novo mutations disturbing the GTP/GDP binding pocket of RAB11B cause intellectual disability and a distinctive brain phenotype. *Am. J. Hum. Genet.* **101**, 824–832 (2017).
39. X. Li, M. DiFiglia, The recycling endosome and its role in neurological disorders. *Prog. Neurobiol.* **97**, 127–141 (2012).
40. Y. Li, B. D. Roy, W. Wang, L. Zhang, L. Zhang, S. B. Sampson, Y. Yang, D.-T. Lin, Identification of two functionally distinct endosomal recycling pathways for dopamine D_2 receptor. *J. Neurosci.* **32**, 7178–7190 (2012).
41. C. Wang, M. Niu, Z. Zhou, X. Zheng, L. Zhang, Y. Tian, X. Yu, G. Bu, H. Xu, Q. Ma, Y. W. Zhang, VPS35 regulates cell surface recycling and signaling of dopamine receptor D1. *Neurobiol. Aging* **46**, 22–31 (2016).
42. N. Ueda, T. Tomita, K. Yanagisawa, N. Kimura, Retromer and Rab2-dependent trafficking mediate PS1 degradation by proteasomes in endocytic disturbance. *J. Neurochem.* **137**, 647–658 (2016).
43. A. Almey, T. A. Milner, W. G. Brake, Estrogen receptors in the central nervous system and their implication for dopamine-dependent cognition in females. *Horm. Behav.* **74**, 125–138 (2015).
44. Q. Huang, D. Zhou, K. Chase, J. F. Gusella, N. Aronin, M. DiFiglia, Immunohistochemical localization of the D1 dopamine receptor in rat brain reveals its axonal transport, pre- and postsynaptic localization, and prevalence in the basal ganglia, limbic system, and thalamic reticular nucleus. *Proc. Natl. Acad. Sci. U.S.A.* **89**, 11988–11992 (1992).

Acknowledgments: We thank J. Lee at Dana Farber Cancer Institute Molecular Biology Core Facilities and R. Tomaino at Harvard Medical School Taplin Mass Spectrometry Core Facility for providing help with mass spectrometry. **Funding:** This work was supported by Endowments from the Pao (Anna Peiqing Sohmen) Foundation to X.L.; M.D. was supported by the Dake Family Fund and the CHDI foundation; Y.K. was a recipient of a scholarship from the Program of Chinese Scholarships Council (201906230074). **Author contributions:** Y.K., M.W., G.C., M.U., Y.L., Y.D., Z.W., X.W., and P.S. designed, performed, and analyzed experiments. Q.Y., M.W., and Z.W. provided histological evaluations and data analysis. Y.K., M.W., M.D., and X.L. wrote the manuscript. X.L. conceived, designed, analyzed, and supervised the overall direction of the study. **Competing interests:** The authors declare that they have no competing interests. **Data and materials availability:** All data needed to evaluate the conclusions in the paper are present in the paper and/or the Supplementary Materials. Additional data related to this paper may be requested from the authors.

Submitted 18 March 2020
Accepted 1 October 2020
Published 18 November 2020
10.1126/sciadv.abb7781

Citation: Y. Ke, M. Weng, G. Chhetri, M. Usman, Y. Li, Q. Yu, Y. Ding, Z. Wang, X. Wang, P. Sultana, M. DiFiglia, X. Li, Trappc9 deficiency in mice impairs learning and memory by causing imbalance of dopamine D1 and D2 neurons. *Sci. Adv.* **6**, eabb7781 (2020).